nature communications

Article

https://doi.org/10.1038/s41467-024-54111-6

VSV$^{\Delta M51}$ drives CD8^{+} T cell-mediated tumour regression through infection of both cancer and non-cancer cells

Received: 11 October 2023

Accepted: 2 November 2024

Published online: 15 November 2024

Check for updates

Jahanara Rajwani[1,2,3], Daniil Vishnevskiy[1,4,5], Madison Turk[1,4,5], Victor Naumenko[1], Chris Gafuik[1,2,3], Dae-Sun Kim[1,2,3,5], Laura K. Mah[1,2,4,5], Shannon Snelling[1,2], Gerone A. Gonzales[3,6], Jingna Xue[4,5], Ayan Chanda[1,3], Kyle G. Potts[1,2], Hayley M. Todesco[1,2], Keith C. K. Lau[5], Karys M. Hildebrand[1,7,8], Jennifer A. Chan[1,9], Shan Liao[4,5], Michael J. Monument[1,7,8], Martin Hyrcza[1,9], Pinaki Bose[1,3,10], Craig N. Jenne[4,5], Johnathan Canton[4,5,6], Franz J. Zemp[1,2,3] & Douglas J. Mahoney[1,2,3,5]

Oncolytic viruses (OV) are designed to selectively infect and kill cancer cells, while simultaneously eliciting antitumour immunity. The mechanism is expected to originate from infected cancer cells. However, recent reports of tumour regression unaccompanied by cancer cell infection suggest a more complex mechanism of action. Here, we engineered vesicular stomatitis virus (VSV)$^{\Delta M51}$-sensitive and VSV$^{\Delta M51}$-resistant tumour lines to elucidate the role of OV-infected cancer and non-cancer cells. We found that, while cancer cell infections elicit oncolysis and antitumour immunity as expected, infection of non-cancer cells alone can also contribute to tumour regression. This effect is partly attributed to the systemic production of cytokines that promote dendritic cell (DC) activation, migration and antigen cross-presentation, leading to magnified antitumour CD8^{+} T cell activation and tumour regression. Such OV-induced antitumour immunity is complementary to PD-1 blockade. Overall, our results reveal mechanistic insights into OV-induced antitumour immunity that can be leveraged to improve OV-based therapeutics.

Oncolytic virus (OV) therapy is a cancer treatment that infuses patients with modified or naturally occurring viruses designed to infect and lyse cancer cells while leaving normal cells intact[1,2]. The first commercial OV to gain regulatory approval was Oncorine (H101), a modified adenovirus approved in China in 2005 for use against advanced nasopharyngeal carcinoma[3]. This was followed by the 2015 FDA approval of Talimogene laherparepvec (T-VEC), a genetically-modified, replication competent herpes simplex virus (HSV), for use in patients with metastatic melanoma[4]. Since then, numerous other OVs have shown clinical activity against multiple tumour types, including

[1]Arnie Charbonneau Cancer Institute; University of Calgary, Calgary, AB T2N 4N1, Canada. [2]Alberta Children's Hospital Research Institute; University of Calgary, Calgary, AB T2N 4N1, Canada. [3]Department of Biochemistry and Molecular Biology, Cumming School of Medicine; University of Calgary, Calgary, AB T2N 4N1, Canada. [4]The Calvin, Joan and Phoebe Snyder Institute for Chronic Disease; University of Calgary, Calgary, AB T2N 4N1, Canada. [5]Department of Microbiology, Immunology, and Infectious Diseases, Cumming School of Medicine; University of Calgary, Calgary, AB T2N 4N1, Canada. [6]Faculty of Veterinary Medicine; University of Calgary, Calgary, AB T2N 4N1, Canada. [7]Department of Surgery, Cumming School of Medicine; University of Calgary, Calgary, AB T2N 4N1, Canada. [8]McCaig Bone and Joint Institute, Cumming School of Medicine; University of Calgary, Calgary, AB T2N 4N1, Canada. [9]Department of Pathology and Laboratory Medicine; University of Calgary, Calgary, AB T2N 4N1, Canada. [10]Department of Oncology; University of Calgary, Calgary, AB T2N 4N1, Canada. e-mail: djmahone@ucalgary.ca

glioblastoma[5], non-muscle-invasive bladder cancer[6], triple-negative breast cancer[7], and hematological malignancies[8].

While the initial premise of OV activity was the selective infection and lysis of tumour cells, accumulating evidence suggests that OVs contribute to tumour regression by promoting antitumour immune responses[1,9]. Although the exact mechanism by which OVs induce antitumour immunity is poorly understood, it is proposed to occur through OV-mediated lysis of cancer cells and the induction of immunogenic cell death (ICD)[10,11]. In this process, infected cancer cells are thought to release damage-associated molecular patterns (DAMP) that enhance presentation of tumour antigens and potentiate the cancer immunity cycle (CIC)[12]. However, ICD-associated DAMPs have only been robustly measured in vitro after OV infection[10,13–15], and have yet to be fully characterized in vivo post virus delivery. Further, this model fails to account for recent studies reporting that OVs can elicit regression of tumours that are poorly infected by virus[16–19]. This has been shown with multiple OV platforms—including HSV, Newcastle disease virus (NDV) and Myxoma virus—using tumours that either naturally do not support productive infection in vivo[20], or have been rendered poorly permissive through genetic modification of tumour lines[16], or pre-immunization of mice[19]. Similar observations have also been made in patients, including in a recent clinical trial testing systemic vesicular stomatitis virus (VSV) for the treatment of relapsed/refractory hematological malignancies. The virus used in this trial encoded the sodium-iodide-symporter (NIS) transgene, allowing in vivo trackability of virus-infected cells. While tumour infection was observed in a non-responding patient, all patients that experienced objective responses had undetectable cancer cell infection[8].

Another observation not accounted for by the ICD model is that OVs have been shown to infect non-malignant cells, despite being designed to selectively infect cancer cells[21–25]. This is perhaps best documented after intravenous (i.v.) administration of VSV, which has been reported to infect non-cancer cells, including endothelial cells, in the tumour microenvironment (TME)[22], as well as immune cells such as B cells, CD169 macrophages and dendritic cells (DC)[26–29], in secondary lymphoid organs (SLO). Importantly, these infections have been shown to contribute to antitumour activity[21,22,26,30]. Thus, understanding the mechanisms by which both cancer and non-cancer cell infections impact OV therapy will undoubtedly reveal new opportunities for improving the treatment's effectiveness. This is especially important for VSV, not only due to its tropism for non-cancer cells after i.v. administration, but also because it is often delivered systemically in clinical trials (clinicaltrials.gov, NCT02923466, NCT03647163, NCT04046445, NCT03017820).

In this study, we sought to determine the role of both cancer and non-cancer cell infections in antitumour activity induced by an oncolytic variant of VSV, called VSV$^{\Delta M51}$, after systemic delivery. Using isogenic mouse tumour models CRISPR-engineered for infection resistance or hypersensitivity, we found that cancer cell infections generate anticancer immunity both locally within the TME and distally within SLOs. Intriguingly, we also found that VSV$^{\Delta M51}$ elicits tumour regression and durable cures in infection-resistant tumour models, suggesting that infection of cancer cells is not the sole driver of therapeutic response. Our results demonstrate that systemically delivered VSV$^{\Delta M51}$ elicits tumour regression through the concerted activity of both cancer and non-cancer cell infections. This finding should help guide ongoing development of safe and effective VSV-based therapeutics for cancer.

Results

VSV$^{\Delta M51}$ elicits regression of infection-resistant tumours

To better understand how systemically delivered VSV$^{\Delta M51}$ elicits immune-mediated tumour rejection, we first sought to determine the relationship between VSV$^{\Delta M51}$ infection of cancer cells and tumour regression using a panel of immunocompetent mouse tumour models. Our panel included the CT-26^{IFNmut} tumour line as a positive control, which is highly permissive to VSV$^{\Delta M51}$ infection due to defects in type I interferon (IFN) signaling[31]. Other cell lines were chosen to represent diverse cancer types (colon, breast, and sarcoma), syngeneic hosts (Balb/c vs C57BL/6), and immunogenicity (low or high). In vitro, all tumour lines were highly susceptible to VSV$^{\Delta M51}$ infection (Supplementary Fig. 1a–f). Interestingly, however, only CT-26^{IFNmut} tumours supported productive VSV$^{\Delta M51}$ infection in vivo after i.v. delivery, as measured by tumour viral titers (Fig. 1a, Supplementary Fig. 1g), or expression of viral transgene products, the latter of which were detected by bioluminescence imaging (BLI; VSV$^{\Delta M51\text{-oFluc}}$) (Fig. 1b) and intravital microscopy (IVM) (Fig. 1c). In all other tumour models, VSV$^{\Delta M51}$ did not productively infect or express transgenes within cancer cells, as measured using the above methods. To further investigate tumour infections in these models, we employed a cre-inducible system, in which cells harbouring a floxed STOP preceding a fluorescent reporter permanently express a fluorescent protein (FP) once infected with cre-expressing VSV$^{\Delta M51}$ (VSV$^{\Delta M51\text{-creGFP}}$; Supplementary Fig. 2a). Importantly, this FP expression is maintained even after viral transgene expression is no longer detectable (Supplementary Fig. 2b–h), allowing more reliable identification of cells that have supported VSV$^{\Delta M51}$ infection. Even when using this model, we rarely observed FP$^+$ cancer cells after i.v. delivery of VSV$^{\Delta M51\text{-creGFP}}$ (Supplementary Fig. 2i), supporting the conclusion that these tumours are not well infected after systemic VSV$^{\Delta M51}$ treatment.

Therapeutically, CT-26^{IFNmut}-bearing mice were cured of their tumours post treatment as expected[31,32], in a manner that was partially dependent on CD8$^+$ T cells (Fig. 1d). However, several other tumour models also underwent significant regression (EMT-6 and M3-9-M) or delayed tumour growth (CT-26^{CL25}) after VSV$^{\Delta M51}$ treatment, despite showing inappreciable virus transgene expression within the tumour. In these models, tumour regression required both CD8$^+$ T cells and replication competent VSV$^{\Delta M51}$, suggesting that infection of non-cancer cells may have the capacity to elicit an antitumour immune response (Fig. 1d).

To more definitively determine whether i.v.-delivered VSV$^{\Delta M51}$ can elicit regression of infection-resistant tumours, we complemented our panel of tumour models with CT-26^{IFNmut} and M3-9-M cell lines genetically engineered for resistance to VSV$^{\Delta M51}$ infection. This was done by functionally ablating the low-density lipoprotein receptor (LDLR) gene family, shown to mediate VSV entry into host cells[33], through CRISPR-inactivation of *Ldlr* and *Lrpap1*. In the CT-26^{IFNmut} cell line, we generated an 'allelic series' of *Ldlr* knockout clones harboring mutations in either zero, one, or two (of four) *Lrpap1* alleles (Supplementary Fig. 3a, b). In vitro, all knockout clones were more resistant to VSV$^{\Delta M51\text{-GFP}}$ infection than parental CT-26^{IFNmut}, with the greatest effect seen in the clone containing the most gene deletions (clone F7; Supplementary Fig. 3c–f). Importantly, resistance to VSV$^{\Delta M51}$ infection was specific, as all knockout clones supported Vaccinia$^{\Delta F4L/\Delta J2R}$ virus infection, an oncolytic poxvirus that does not use the LDLR family for viral entry (Supplementary Fig. 3g–i).

In vivo, both by IVM (Fig. 1e, Supplementary Fig. 3j) and BLI (Fig. 1f, Supplementary Fig. 3k), only the F7 clone was resistant to VSV$^{\Delta M51}$ infection, demonstrating that mutations in 100% of *Ldlr* alleles and at least 50% of *Lrpap1* alleles are sufficient to abrogate cancer cell infection in vivo. Consistent with our experiments in naturally resistant tumours (Fig. 1d), F7-bearing mice underwent significant tumour regression with systemic VSV$^{\Delta M51}$ treatment (Fig. 1g). These responses were CD8$^+$ T cell dependent, confirming VSV$^{\Delta M51}$-mediated engagement of antitumour immunity despite severe impairment of cancer cell infection.

To validate these results in an additional tumour model established on a different mouse background, we carried out a similar approach in the M3-9-M cell line. Although M3-9-M tumours do not support measurable VSV$^{\Delta M51}$ infection in vivo (Fig. 1a–c, Supplementary

https://doi.org/10.1038/s41467-024-54111-6

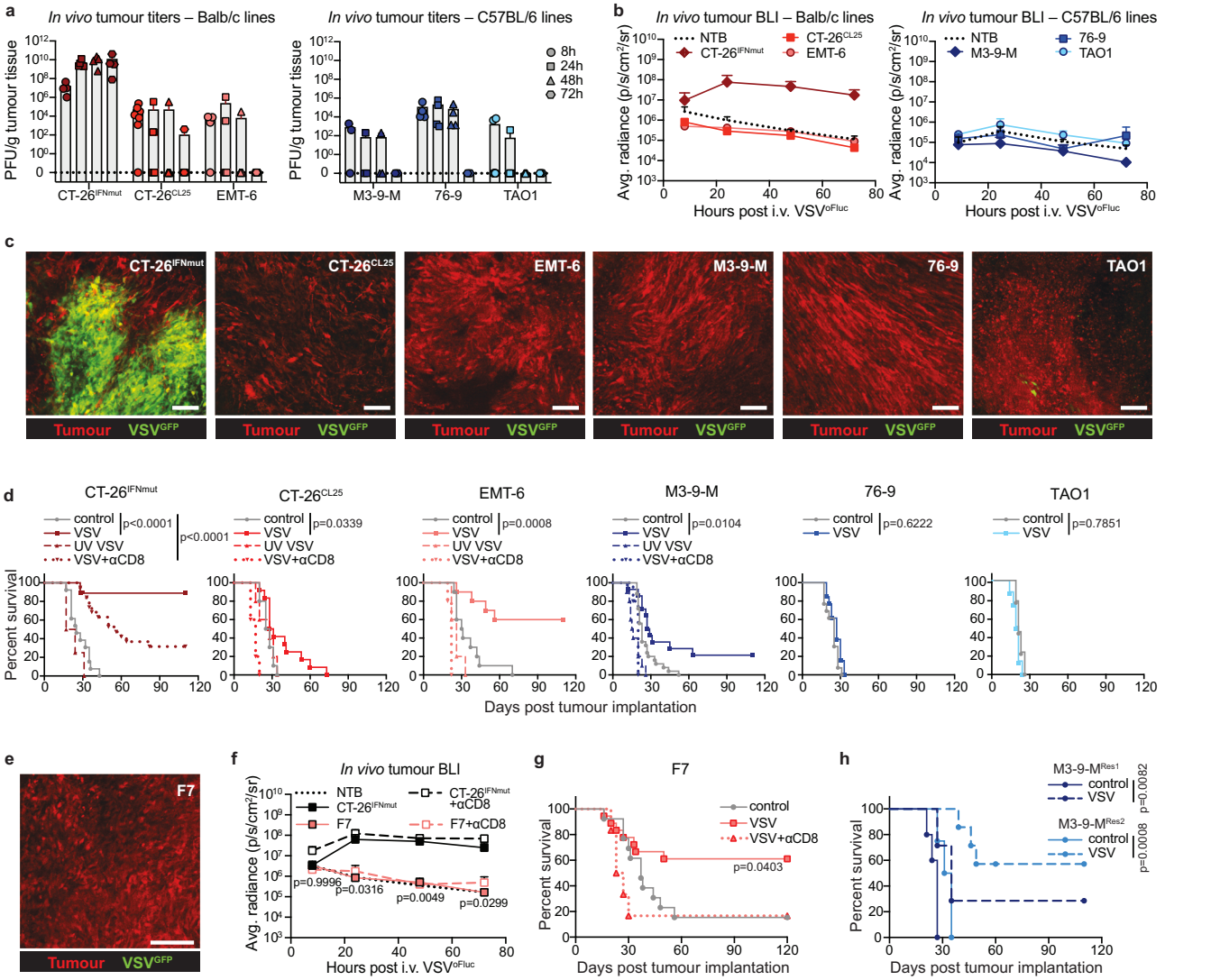

Fig. 1 | VSV$^{\Delta M51}$ elicits tumour regression in infection-resistant tumours. **a** Tumour virus titers post VSV$^{\Delta M51\text{-}GFP}$ ($n = 3$–7 mice/group, compiled from 1 or 2 independent experiments). **b** Viral transgene expression in tumours post VSV$^{\Delta M51\text{-}oFluc}$ ($n = 3$–5 mice/group measured repeatedly over time, except non-tumour bearing (NTB), which had 2–3 mice/group, representative of 2 independent experiments). **c** Tumour infection 24 h post VSV$^{\Delta M51\text{-}GFP}$, representative of $n = 4$ mice/group imaged over 2 independent experiments. Scale bars are 100 μm. **d** Overall survival of tumour-bearing mice treated with infectious or UV-irradiated VSV$^{\Delta M51}$ ± CD8 neutralizing antibodies (αCD8, $n = 4$–25 mice/group, compiled from 2–3 independent experiments, log-rank Mantel–Cox test). **e** Infection in F7 tumours 24 h post VSV$^{\Delta M51\text{-}GFP}$, representative of $n = 6$ mice imaged over 2 independent experiments. Scale bar is 300 μm. **f** Viral transgene expression in tumours post VSV$^{\Delta M51\text{-}oFluc}$ ± αCD8 ($n = 6$ mice/group (CT-26^{IFNmut} + αCD8, F7 + αCD8), $n = 7$ mice/group (CT-26^{IFNmut}), $n = 10$ mice/group (F7), $n = 3$ mice/group (NTB) measured repeatedly over time, representative of 2 independent experiments, two-way ANOVA with Dunnett's post-test comparing F7 to CT-26^{IFNmut}). **g** Overall survival of mice bearing F7 tumours post VSV$^{\Delta M51}$ ± αCD8 ($n = 13$ mice/group (control), $n = 17$ mice/group (VSV), $n = 6$ mice/group (VSV + αCD8), compiled from 2 independent experiments, log-rank Mantel–Cox test of VSV$^{\Delta M51}$ compared to control). **h** Overall survival of mice bearing infection-resistant M3-9-M tumours post VSV$^{\Delta M51}$ ($n = 5$ mice (M3-9-M^{Res1} control), $n = 4$ mice (M3-9-M^{Res2} control), $n = 7$ mice (M3-9-M^{Res1} VSV, M3-9-M^{Res2} VSV), representative of 2 independent experiments, log-rank Mantel-Cox test). Unless otherwise indicated, VSV$^{\Delta M51}$ was delivered i.v. at 5×10^8 PFU. Bars/points at mean ± SD. Source data are provided as a Source Data file. Occasionally n is given as a range as the number of mice in each group varies. Please see the Source Data file for the exact n in each group.

Fig. 2i), we nonetheless generated two knockout clones containing mutations in all *Ldlr* alleles and ~50% of *Lrpap1* alleles (M3-9-M^{Res1} and M3-9-M^{Res2}; Supplementary Fig. 3l, m) to ensure infection resistance. Similar to CT-26^{IFNmut} knockout clones, M3-9-M knockout clones were also specifically protected from VSV$^{\Delta M51\text{-}GFP}$ infection in vitro (Supplementary Fig. 3n–t) and did not support measurable infection in vivo (Supplementary Fig. 3u). Further, mice bearing infection-resistant M3-9-M tumours responded similarly to VSV$^{\Delta M51\text{-}GFP}$ as parental M3-9-M-bearing mice (Fig. 1d, h).

Taken together, these data suggest that productive infection within cancer cells is not a strict requirement for immune-mediated tumour regression after systemic VSV$^{\Delta M51}$ treatment, supporting a growing appreciation for the role of both cancer and non-cancer cell infections in OV therapy.

Cancer cell infections elicit both local and abscopal tumour control

We next sought to identify tumour characteristics that impact responsiveness to VSV$^{\Delta M51}$ therapy. We noted that tumour models exhibiting significant regression after VSV$^{\Delta M51}$ treatment (CT-26^{CL25}, EMT-6, M3-9-M) were reported to be 'hot', or immunogenic[20,29,34–36], while non-responsive tumour models (76-9, TAO1) were reported to be 'cold', or non-immunogenic[20,34,36,37]. We therefore asked whether immunogenicity impacts responsiveness to VSV$^{\Delta M51}$ therapy. To

investigate this, we used the M3-9-M model, which is derived from male mice and expresses H-Y histocompatibility antigens reported to be immunogenic in female hosts[20,34,36]. To confirm this model, we treated mice bearing M3-9-M tumours with PD-1 blockade therapy and found that nearly 100% of female mice were cured of their tumours, whereas all male mice succumbed to their disease (Fig. 2a). Further, M3-9-M tumours in female mice were more infiltrated with $CD8^+$ T cells (Fig. 2b). To control for potential sex differences in anticancer immunity[38], we engineered an M3-9-M cell line to express the model antigen, chicken ovalbumin (OVA; M3-9-M^{OVA}). As expected, this rendered tumours immunogenic in male mice (Fig. 2a, b). When mice bearing these tumours were treated systemically with $VSV^{\Delta M51}$, we found that, while all tumour models were similarly unsupportive of productive virus infection in vivo (Fig. 2c), only immunogenic tumours regressed after treatment (Fig. 2d). This demonstrates that tumour immunogenicity is a critical factor for responsiveness to systemically-delivered $VSV^{\Delta M51}$.

Given that OVs are thought to increase tumour immunogenicity by eliciting ICD through viral oncolysis[10,11], we next asked whether cancer cell infections, when present, improve antitumour immunity. Indeed, although the $CD8^+$ T cell-independent tumour responses in the CT-26^{IFNmut} model demonstrate that cancer cell infections may cause direct tumour regression (Fig. 1d), they do not indicate whether they can also promote antitumour immunity. Further, as CT-26^{IFNmut} is our only tumour model supporting productive infection in vivo, it is unclear whether cancer cell infections can contribute to tumour regression in other models. To address this, we genetically engineered M3-9-M cells to be hypersensitive to $VSV^{\Delta M51}$ infection, by ablating the IFNα/β receptor (IFNAR1), a critical component of the type I IFN-induced antiviral signaling cascade[39]. Two CRISPR-inactivated *Ifnar1* knockout clones were selected, M3-9-M^{Sens1} and M3-9-M^{Sens2} (Supplementary Fig. 4a), based on in vitro evidence of infection hypersensitivity and loss of responsiveness to type I IFNs (Supplementary Fig. 4b–d). When implanted into mice, M3-9-M^{Sens1} and M3-9-M^{Sens2} were more sensitive to $VSV^{\Delta M51}$ infection than parental M3-9-M, as measured by IVM (Fig. 2e) and BLI (Fig. 2f, Supplementary Fig. 4e).

As expected, enabling tumour infection in this model improved therapeutic efficacy, with 100% of M3-9-M^{Sens1}- or M3-9-M^{Sens2}-bearing mice showing complete and durable tumour responses (Fig. 2g–i). Importantly, these responses were $CD8^+$ T cell-dependent, as $VSV^{\Delta M51}$-treatment of $CD8^+$ T cell-depleted mice generated only transient tumour regression (Fig. 2g–i). To determine whether tumour regression required $CD8^+$ T cells to enter the TME from the tumour draining lymph node (TdLN), we treated M-3-9M^{Sens1} tumour-bearing mice with FTY-720, a drug that sequesters lymphocytes in the lymph node (LN)[40] (Supplementary Fig. 4f, g). Interestingly, ~70% of mice treated with $VSV^{\Delta M51}$ and FTY-720 were cured of their primary tumours (Supplementary Fig. 4h), suggesting that productive tumour infection can generate local tumour control without recruiting T cells from SLOs. Given that durable cures are dependent on $CD8^+$ T cells (Fig. 2g–i), this local control presumably occurs through the engagement of pre-existing T cells within the TME. However, 50% of mice still succumbed from disease, mostly due to the development of lung metastases (accounting for 5/7 deaths; Supplementary Fig. 4h, i). This suggests that systemic tumour control requires additional $CD8^+$ T cell support from SLOs.

We next asked whether cancer cell infections can enhance antitumour T cell activity in a model of low tumour immunogenicity. To test this, we implanted M3-9-M^{Sens1} into male mice and treated them with $VSV^{\Delta M51}$. While $CD8^+$ T cell depletion alone did not impact tumour growth, suggesting that $CD8^+$ T cells do not contribute to tumour control in the steady state of this low immunogenicity tumour, $VSV^{\Delta M51}$-treated mice experienced significant $CD8^+$ T cell-dependent tumour regression (Fig. 2j). This suggests that cancer cell infections can potentiate antitumour $CD8^+$ T cell-mediated immunity even against poorly immunogenic tumours.

And finally, to investigate whether cancer cell infections can elicit abscopal anticancer immunity against distant non-infected tumours, we implanted mice on contralateral flanks, such that they bore either two infection-sensitive tumours (M3-9-M^{Sens1} uniform bilateral), two infection-resistant tumours (M3-9-M^{Res1} uniform bilateral), or one of each (mixed bilateral; Fig. 2k). While M3-9-M^{Sens1} tumours were similarly responsive to $VSV^{\Delta M51}$ treatment in all groups (Fig. 2l), M3-9-M^{Res1} tumours underwent greater tumour regression when the contralateral tumour was infectable (mixed bilateral) rather than resistant (M3-9-M^{Res1} uniform bilateral) (Fig. 2m, n). Importantly, M3-9-M^{Res1} tumours remained resistant to infection even in the presence of a contralateral infectable tumour (Supplementary Fig. 4j).

Collectively, these data suggest that cancer cell infections can generate both local and systemic antitumour immunity by engaging CD8 T^+ cells within the TME and SLOs.

Non-cancer cell infections stimulate ongoing anticancer immunity

Given that $VSV^{\Delta M51}$ can generate $CD8^+$ T cell-mediated antitumour activity without productively infecting and spreading through the tumour (Fig. 1), we next sought to understand how virus infection within non-cancer cells elicits tumour regression, by performing experiments in mice bearing infection-resistant M3-9-M^{Res1} tumours. To begin, we asked whether infection of non-cancer cells leads to anticancer $CD8^+$ T cell accumulation in tumours. Indeed, we found that $VSV^{\Delta M51}$ treatment of OVA-expressing M3-9-M^{Res1} (M3-9-$M^{Res1/OVA}$)-bearing mice led to an increased number of OVA-specific $CD8^+$ T cells within the tumour (Fig. 3a, Supplementary Fig. 5a), suggesting that $VSV^{\Delta M51}$ treatment enhances antitumour $CD8^+$ T cell responses. To determine whether $VSV^{\Delta M51}$ treatment of infection-resistant tumours improves T cell activity in the TME or TdLN, mice bearing M3-9-M^{Res1} were treated with $VSV^{\Delta M51}$ in the presence or absence of FTY-720. Interestingly, $VSV^{\Delta M51}$ no longer elicited durable cures if T cell egress from LNs was blocked with FTY-720 (Fig. 3b, c). This suggests that virus replication within non-cancer cells enhances anticancer immunity by acting predominantly on $CD8^+$ T cells in the TdLN.

One way non-cancer cell infections could engage $CD8^+$ T cells in the TdLN is by enhancing tumour antigen presentation[12]. Indeed, systemic $VSV^{\Delta M51}$ treatment of M3-9-M^{Res1}-bearing mice increased the number of $CD11c^+$ DCs and $CD103^+$ classical DCs (cDC1) in the TdLN, as well as their expression of the costimulatory markers, CD80 and CD86 (Fig. 3d, e). This coincided with a decrease in the number of $CD11c^+$ DCs within the tumour (Fig. 3f). Further, DCs that remained in the tumour had upregulated expression of CD80, CD86 (Fig. 3g), and the LN-homing chemokine receptor, CCR7 (Fig. 3h). This suggests that $VSV^{\Delta M51}$ infection of predominantly non-cancer cells can promote DC activation and their migration from the tumour to the TdLN. To study this further, we engineered M3-9-M^{Res1} to express mCherry (M3-9-$M^{Res1/mCherry}$), enabling us to track DCs carrying tumour-derived antigen[41] (Supplementary Fig. 5b, c). $VSV^{\Delta M51}$ treatment significantly increased the number of $mCherry^+$DCs in the TdLN (Fig. 3i), and concurrently decreased the number of $mCherry^+$DCs in the tumour (Fig. 3j), suggesting that virus treatment enhances trafficking of antigen presenting cells (APC) from the tumour to the TdLN. Further, we found that $Batf3^{-/-}$ mice, which lack cross-presenting cDC1 populations[42], were refractory to $VSV^{\Delta M51}$-induced M3-9-M^{Res1} tumour regression (Fig. 3k). This demonstrates that cDC1 cells are a critical component of the antitumour immune response engaged by $VSV^{\Delta M51}$ infection of non-cancer cells.

To determine whether non-cancer cell infections enhance antigen-specific $CD8^+$ T cell activation in the LN, we adoptively transferred naïve OT-I cells into mice bearing either M3-9-M^{Res1} or

https://doi.org/10.1038/s41467-024-54111-6

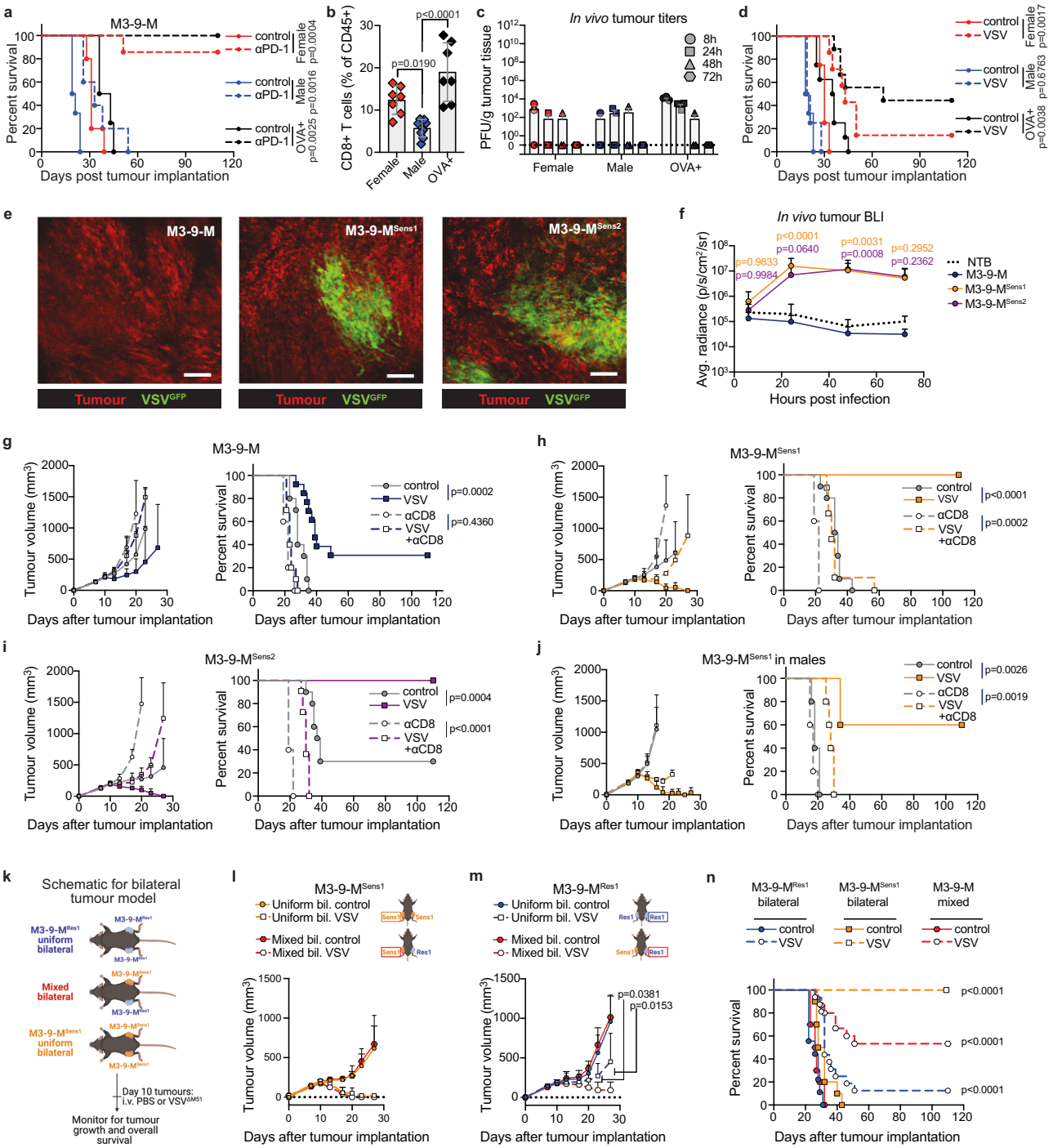

Fig. 2 | Cancer cell infections generate local tumour control and distant abscopal immunity. a Overall survival of tumour-bearing mice treated with PBS or anti-PD-1 ($n = 5$ mice/group, except $n = 7$ mice/group (Female anti-PD-1), $n = 6$ mice/group (Male control), $n = 4$ mice/group (OVA+ control), representative of 2 independent experiments, log-rank Mantel-Cox test). **b** $CD8^+$ T cell frequency in M3-9-M tumours 10 days post-implantation ($n = 7$ mice/group (Female, OVA +), $n = 9$ mice/group (Male), compiled from 2 independent experiments, one-way ANOVA with Tukey's post-test). **c** M3-9-M tumour virus titers post $VSV^{\Delta M51\text{-}GFP}$ ($n = 3$ mice/group, representative of 2 independent experiments). **d** Overall survival of M3-9-M tumour-bearing mice treated with PBS or $VSV^{\Delta M51\text{-}GFP}$ ($n = 4$–9 mice/group, compiled from 1 or 2 independent experiments, log-rank Mantel-Cox test). **e** Tumour infection 24 h post $VSV^{\Delta M51\text{-}GFP}$, representative of $n = 4$ mice/group imaged over 2 independent experiments. Scale bars are 100 μm. **f** Viral transgene expression in tumours post $VSV^{\Delta M51\text{-}oFluc}$ ($n = 8$–12 mice/group measured repeatedly over time, except NTB, which had 3–6 mice, compiled from 2 independent experiments, two-way ANOVA with Dunnett's post-test comparing indicated tumours to M3-9-M). **g**–**j** Tumour growth (left) and overall survival (right) of tumour-bearing mice after treatment with PBS or $VSV^{\Delta M51} \pm \alpha CD8$ (left: $n = 5$ mice/group (except $n = 4$ mice/group for VSV + αCD8 condition in **g**), representative of 2 independent experiments; right: $n = 5$–13 mice/group, compiled from 1–2 independent experiments, log-rank Mantel–Cox test). **k** Schematic of experiment involving bilateral infection-modulated tumours. **l**, **m** Tumour growth of M3-9-M^{Sens1} (**l**) or M3-9-M^{Res1} (**m**) tumours after PBS or $VSV^{\Delta M51}$ treatment of mice bearing bilateral tumours ($n = 5$–16 tumours/group, representative of 2 independent experiments, two-way ANOVA with Tukey's post-test). **n** Overall survival of mice bearing bilateral tumours treated with PBS or $VSV^{\Delta M51}$ ($n = 9$–16 mice/group, compiled from 2 independent experiments, log-rank Mantel-Cox test). In all experiment, $VSV^{\Delta M51}$ was delivered i.v. at 5×10^8 PFU. Points at mean ± SD. Schematics in Fig. 2k–m were created in BioRender. Lab, M (2024) BioRender.com/m62j741. Source data are provided as a Source Data file. Occasionally n is given as a range as the number of mice in each group varies. Please see the Source Data file for the exact n in each group.

https://doi.org/10.1038/s41467-024-54111-6

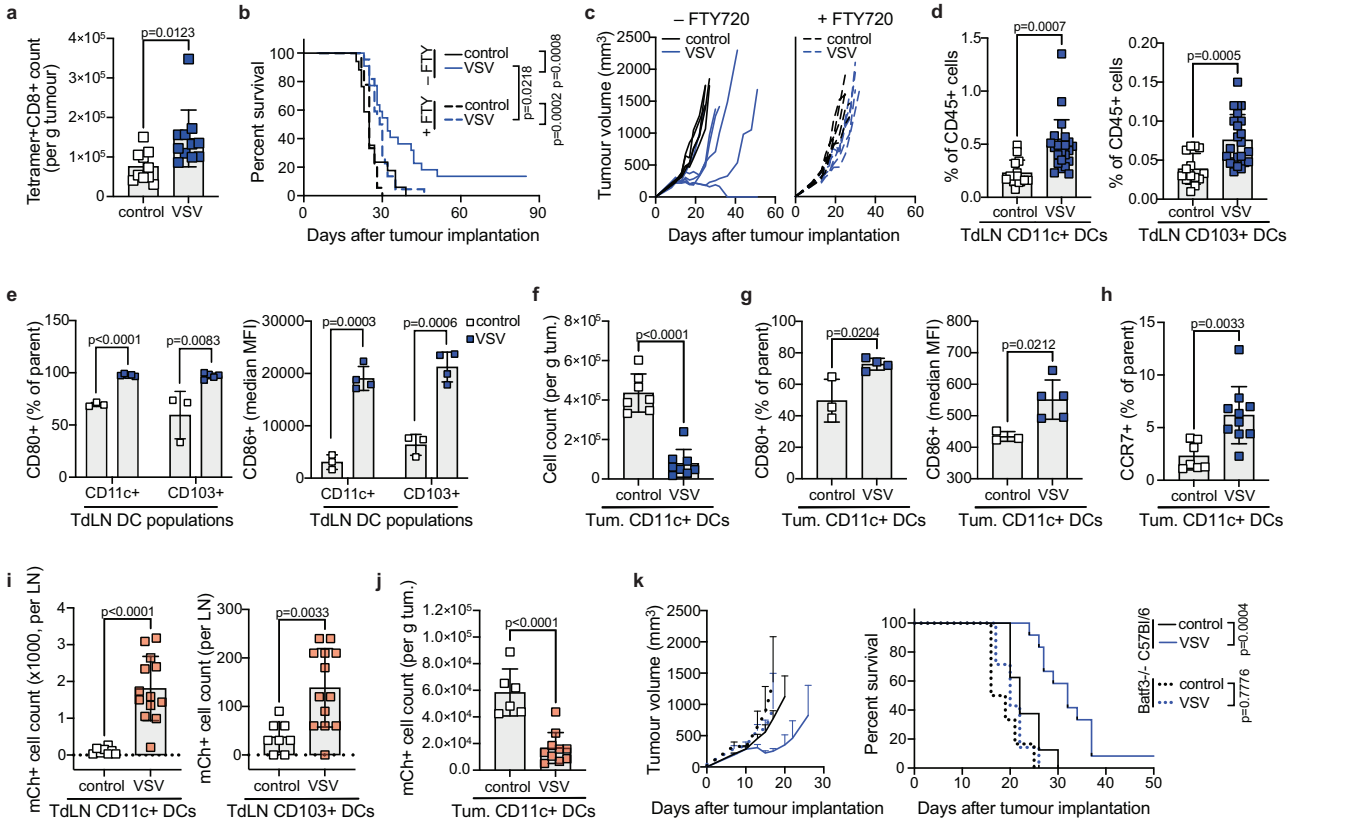

Fig. 3 | Non-cancer cell infections promote DC activation and migration to the TdLN. a OVA-specific CD8$^+$ T cell count in M3-9-M$^{Res1/OVA}$ tumours 6 days post VSV$^{\Delta M51}$ ($n = 10$ mice/group (control), $n = 11$ mice/group (VSV), compiled from 2 independent experiments, two-tailed, unpaired t test). **b** Overall survival of M3-9-M^{Res1}-bearing mice treated with PBS/VSV$^{\Delta M51}$ ± FTY-720 ($n = 17$-22 mice/group, compiled from 3 independent experiments, log-rank Mantel-Cox test). **c** Tumour growth of mice in **b** ($n = 5$ mice/group (control), $n = 6$ mice/group (VSV), representative of 3 independent experiments). **d** Frequency of total DCs (left) and CD103$^+$ DCs (right) of CD45$^+$ cells in the TdLN of M3-9-M^{Res1}-bearing mice 24 h post PBS/VSV$^{\Delta M51}$ ($n = 14$ mice/group (control), $n = 23$ mice/group (VSV), compiled from 4 independent experiments, two-tailed, unpaired t test). **e** Expression of CD80 (left) and CD86 (right) on TdLN DCs of mice treated as in **d** ($n = 3$–5 mice/group, representative of 4 independent experiments, multiple two-tailed unpaired t tests with Holm-Sidak post-test). **f**–**h** Count (**f**) and expression of CD80 (**g**; left), CD86 (**g**; right) or CCR7 (**h**) on DCs in tumours of mice treated as in **d** (for **f**, **h**: $n = 7$–10 mice/group, compiled from 2 independent experiments; for **g**: $n = 3$–5 mice/group, representative of 2 independent experiments; two-tailed, unpaired t test). **i**, **j** Count of mCherry$^+$ total DCs (left) and mCherry$^+$CD103$^+$ DCs (right) in TdLNs (**i**) or tumours (**j**) of M3-9-M$^{Res1/mCherry}$-bearing mice 24 h post PBS/VSV$^{\Delta M51}$ ($n = 6$–13 mice/group, compiled from 2 independent experiments, two-tailed, unpaired t test). **k** Tumour growth (left) and overall survival (right) of M3-9-M^{Res1}-bearing C57BL/6 or Batf3−/− mice post VSV$^{\Delta M51}$ (left: $n = 3$–6 mice/group, representative of 2 independent experiments; right: $n = 6$–12 mice/group, compiled from 2 independent experiments, log-rank Mantel-Cox test). In all experiment, VSV$^{\Delta M51}$ was delivered i.v. at 5×10^8 PFU. Points/bars at mean ± SD. Occasionally n is given as a range as the number of mice in each group varies. Please see the Source Data file for the exact n in each group.

M3-9-M$^{Res1/OVA}$ tumours (Supplementary Fig. 6a, b). Interestingly, VSV$^{\Delta M51}$ significantly increased OT-I cell frequencies in the TdLN of OVA-positive tumours (Fig. 4a, b), but not in non-draining SLOs (Supplementary Fig. 6c, d). Further, OT-I cells did not proliferate in the absence of OVA, even with VSV$^{\Delta M51}$ treatment (Fig. 4a, b). Importantly, this was not due to initial differences in OT-I cell trafficking between LNs draining OVA$^+$ and OVA$^-$ tumours. Indeed, in mice bearing contralateral M3-9-M^{Res1} and M3-9-M$^{Res1/OVA}$ tumours, OT-I cells homed equally between TdLNs (Supplementary Fig. 6e, f). This was measured 24 hours post adoptive transfer, early enough that OT-I cells had not yet proliferated (Supplementary Fig. 6g), despite recognizing cognate antigen in OVA-draining LNs, as measured by CD69$^+$ expression (Supplementary Fig. 6h). These data suggest that virus replication predominantly within non-cancer cells specifically potentiates anti-tumour CD8$^+$ T cell activation within an ongoing immune response, likely by enhancing upstream DC function.

Finally, given the recent discovery that PD-1 blockade works in part by improving T cell priming in the TdLN[43,44], we asked whether this therapy is enhanced by VSV$^{\Delta M51}$ treatment. As M3-9-M is immunogenic and highly responsive to PD-1 blockade (Fig. 2a), we used a sub-curative dose to treat tumour-bearing mice (Fig. 4c). Combining PD-1 blockade with systemic VSV$^{\Delta M51}$ resulted in enhanced T cell activation within the TdLN (Fig. 4d) and significantly improved tumour control (Fig. 4e). We therefore speculate that PD-1 blockade and systemic VSV$^{\Delta M51}$ treatment may act synergistically in the TdLN to promote anticancer CD8$^+$ T cell functioning.

Overall, these data demonstrate that virus replication within non-cancer cells has an adjuvant effect on ongoing anticancer immune responses by promoting DC activation and migration to the TdLN and the subsequent activation and tumour trafficking of anticancer CD8$^+$ T cells.

VSV$^{\Delta M51}$ infection of the TdLN promotes DC activation

We next sought to understand how VSV$^{\Delta M51}$ infection of non-cancer cells enhances DC activation and migration to the LN. For these studies, we modeled immunogenic tumours with the FITC skin painting technique, as it allows DCs that have engulfed FITC in a locally inflamed environment to be easily tracked by flow cytometry as they migrate to the draining lymph node (dLN)[45] (Fig. 5a). As anticipated, systemic VSV$^{\Delta M51}$ treatment enhanced the migration of FITC$^+$ DCs (CD11c$^+$ and CD103$^+$) to the dLN (Fig. 5b, Supplementary Fig. 7). Further, it increased expression of CD80 and CD86 on FITC$^+$ DCs (Fig. 5c, d),

https://doi.org/10.1038/s41467-024-54111-6

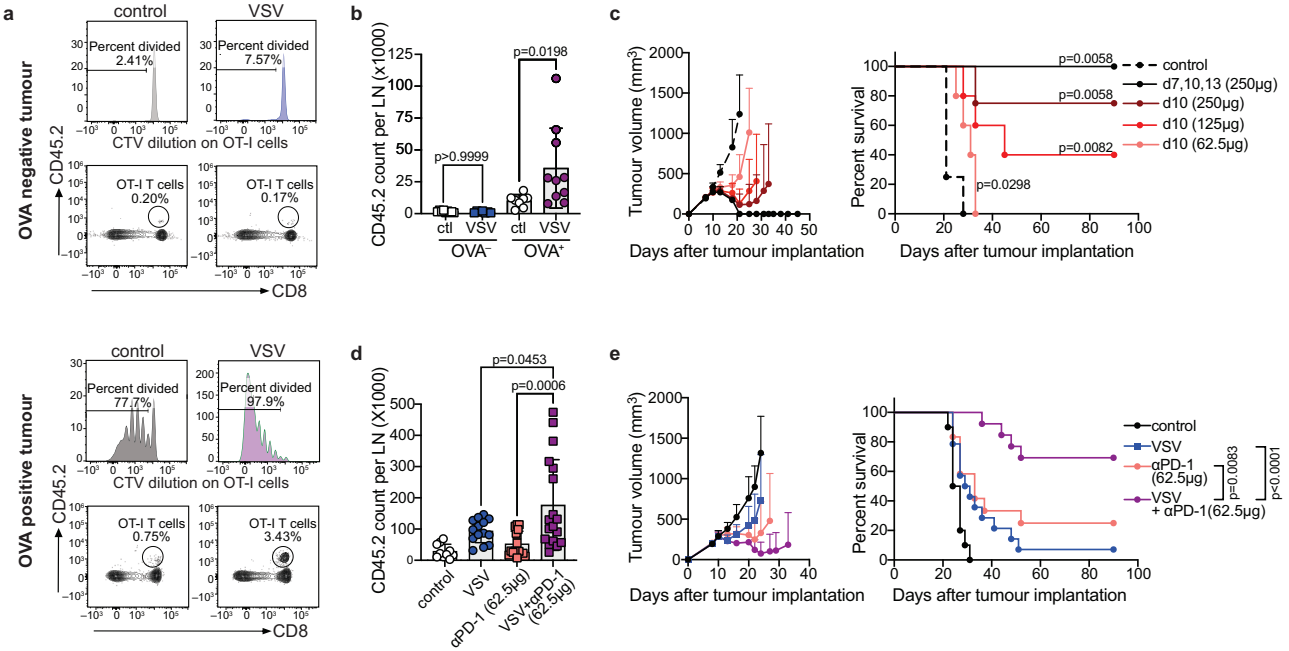

Fig. 4 | Non-cancer cell infections enhance activation of antitumour CD8⁺ T cells. a Representative flow cytometry plots of CTV dilution (top) and OT-I frequency among CD45⁺ cells (bottom) in TdLNs of M3-9-M^{Res1}- or M3-9-M$^{Res1/OVA}$-bearing mice after transfer of OT-I cells ± VSV$^{\Delta M51}$. **b** Count of OT-I cells in TdLNs of mice treated as in **a** ($n = 7$–10 mice/group, compiled from three independent experiments, one-way ANOVA with Tukey's post-test). **c** Tumour growth (left) and overall survival (right) of M3-9-M^{Res1}-bearing mice treated with anti-PD-1 ($n = 4$ mice/group except $n = 5$ mice/group (d10 (125 μg), d10 (62.5 μg)), representative of 2 independent experiments, log-rank Mantel-Cox test on overall survival). **d** OT-I cell count in TdLNs of M3-9-M$^{Res1/OVA}$-bearing mice, post OT-I transfer and VSV$^{\Delta M51}$ and/or anti-PD-1 treatment (62.5 μg on day 10) ($n = 10$–18 mice/group, compiled from 3 independent experiments, one-way ANOVA with Tukey's post-test). **e** Tumour growth (left) and overall survival (right) of M3-9-M^{Res1}-bearing mice treated as in **d** (left: $n = 5$ mice/group (control, αPD-1 (62.5 μg)), $n = 7$ mice/group (VSV, VSV + αPD-1 (62.5 μg)); right: $n = 10$–14 mice/group, compiled from 2 independent experiments, log-rank Mantel-Cox test). In all experiment, VSV$^{\Delta M51}$ was delivered i.v. at 5×10^8 PFU. Points/bars at mean ± SD. Occasionally n is given as a range as the number of mice in each group varies. Please see the Source Data file for the exact n in each group.

making this a suitable and convenient model to test factors influencing VSV$^{\Delta M51}$-induced activation and trafficking of DCs.

Having previously demonstrated that mouse LNs represent major reservoirs of VSV$^{\Delta M51}$ infection after systemic delivery[28,29] (Supplementary Fig. 8a), we hypothesized that these infections were responsible for the enhanced recruitment of DCs. Interestingly, these infections co-localize with CD169⁺ macrophages (Supplementary Fig. 8b), which are typically thought to be infected via the afferent lymphatics following subcutaneous delivery of VSV[46]. Surprisingly, we found that LN infections after systemic delivery also required intact afferent lymphatics, as suturing afferent lymphatic vessels[47] prior to i.v. VSV$^{\Delta M51}$ administration blocked infection of the dLN (Fig. 5e, f). This suggests a yet-to-be-determined mechanism of entry whereby virus particles enter the LNs via the subcapsular sinus (SCS), despite being delivered intravenously.

Importantly, this discovery allowed us to determine the contribution of VSV$^{\Delta M51}$ infection in the dLN to DC biology, as it informed us that LN infection after subcutaneous delivery may mimic infection of the LN achieved after systemic administration. In this approach, we delivered virus to the right lower flank, as it drains to the inguinal lymph node (iLN), similar to M3-9-M tumours and FITC painted skin. We found that subcutaneous delivery of 5×10^8 plaque forming units (PFU) of VSV$^{\Delta M51}$ resulted in similar LN infection (Supplementary Fig. 8c) and cytokine/chemokine levels (Supplementary Fig. 8d) as 5×10^8 PFU delivered systemically, without leaking to systemic sites (Supplementary Fig. 8e). Having established the dose of subcutaneous VSV$^{\Delta M51}$ required to emulate LN infection after systemic delivery, we next asked whether infection of the LN alone could induce recruitment of DCs in the FITC painting model. Interestingly, DC migration was unaffected by LN infection (Fig. 5g), although costimulatory marker expression was increased to similar levels as with systemic treatment (Fig. 5h, i). Nonetheless, in tumour-bearing mice, subcutaneous VSV$^{\Delta M51}$ injections alone were insufficient to provide a survival benefit (Fig. 5j), suggesting that non-cancer cell infections elsewhere are required for mounting therapeutically meaningful VSV$^{\Delta M51}$-induced antitumour immunity.

Collectively, these data suggest that VSV$^{\Delta M51}$ infection of cells within the TdLN promotes DC activation, which alone is insufficient to generate tumour regression in mice.

VSV$^{\Delta M51}$-induced serum factors promote tumour antigen presentation

As systemically delivered VSV interacts with cells in many organs[26–29,32], we hypothesized that these infected sites secrete factors into the serum that influence DC function. To test this, we treated FITC painted mice with serum harvested from mice treated for 6 or 12 hours with VSV$^{\Delta M51}$. Compared to control serum, VSV$^{\Delta M51}$-conditioned serum increased total FITC⁺ DC recruitment to the dLN (Supplementary Fig. 9a), although unsurprisingly to a lesser extent than delivery of replication-competent VSV$^{\Delta M51}$. We thus sought to identify the factors that contributed to DC recruitment to the LN. Through multiplex ELISA, we found that numerous cytokines and chemokines were upregulated 6 and 12 hours post VSV$^{\Delta M51}$ infection (Supplementary Fig. 9b), but chose to focus on TNF and type I IFNs, as these have previously been implicated in DC function[48,49]. Strikingly, inhibiting the activity of these cytokines abrogated the VSV$^{\Delta M51}$-induced recruitment of FITC⁺ DCs to the dLN in the FITC painting model (Fig. 6a). Further, FITC⁺ DCs had significantly reduced expression of CD80 and CD86 (Fig. 6b, c), suggesting that TNF and type I IFNs contribute to VSV$^{\Delta M51}$-induced upregulation of costimulatory markers on DCs. Similarly, in

https://doi.org/10.1038/s41467-024-54111-6

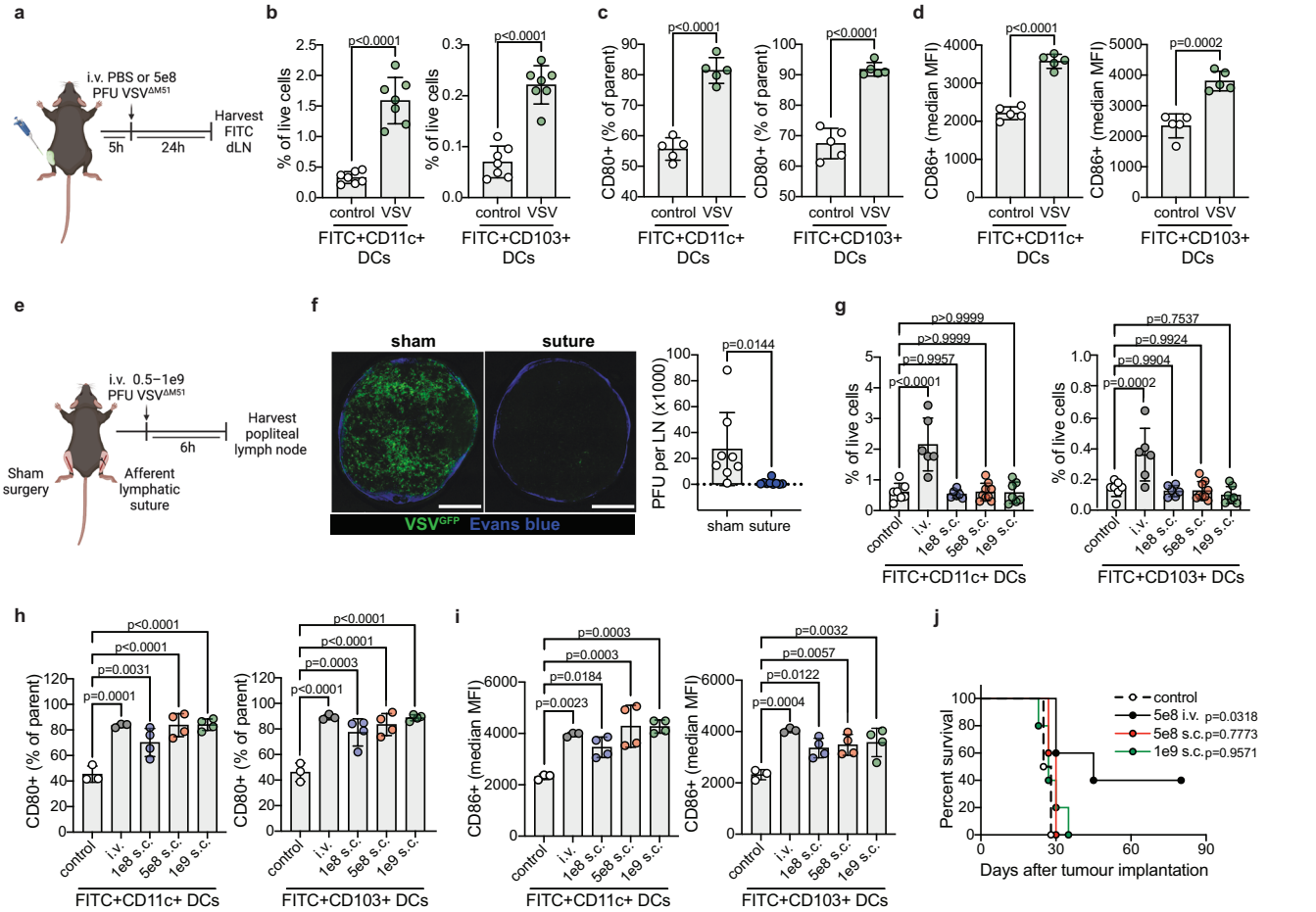

Fig. 5 | VSV$^{\Delta M51}$ infection of the TdLN promotes DC activation. a Schematic of FITC painting technique. **b** Frequency of FITC$^+$ DCs (left) and FITC$^+$CD103$^+$ DCs (right) in the iLN after FITC painting depicted in **a** ($n = 7$ mice/group, compiled from three independent experiments, two-tailed, unpaired t test). **c**, **d** Expression of CD80 (**c**) and CD86 (**d**) on FITC$^+$ DCs (left) and FITC$^+$CD103$^+$ DCs (right) in the iLN after FITC painting depicted in **a** ($n = 5$ mice/group, compiled from 2 independent experiments, two-tailed, unpaired t test). **e** Schematic of afferent lymphatic suture experiment. **f** Representative ex vivo images (left) and virus titers (right) in the popliteal LN after lymphatic suture and VSV$^{\Delta M51\text{-}GFP}$ delivery (5×10^8–1×10^9 PFU delivered i.v.) (left: scale at 300 μm; right: $n = 8$ mice/group (sham), $n = 9$ mice/group (suture), compiled from 2 independent experiments, two-tailed, unpaired t test). **g** Frequency of total FITC$^+$ DCs (left) and FITC$^+$CD103$^+$ DCs (right) in the iLN of FITC painted mice 24 h post VSV$^{\Delta M51}$ ($n = 6$–9 mice/group, compiled from 3 independent experiments, one-way ANOVA with Dunnett's post-test). **h**, **i** Expression of CD80 (**h**) or CD86 (**i**) on total FITC$^+$ DCs (left) and FITC$^+$CD103$^+$ DCs (right) in the iLN of mice treated as in **g** ($n = 4$ mice/group except $n = 3$ mice/group (control, i.v.), representative of 3 independent experiments, one-way ANOVA with Dunnett's post-test). **j** Overall survival of M3-9-M^{Res1}-bearing mice post VSV$^{\Delta M51}$ ($n = 5$ mice/group except $n = 4$ mice/group (control), log-rank Mantel–Cox test between treatment groups and control). Unless otherwise indicated, VSV$^{\Delta M51}$ was delivered i.v. at 5×10^8 PFU. Bars at mean ± SD. For each subfigure showing data for both CD11c$^+$ cells and CD103$^+$ cells, the same samples were used to measure CD11c and CD103. Schematics in **a** and **e** were created in BioRender. Lab, M (2024) BioRender.com/m62j741. Source data are provided as a Source Data file. Occasionally n is given as a range as the number of mice in each group varies. Please see the Source Data file for the exact n in each group.

the M3-9-M$^{Res1/mCherry}$ tumour model, neutralization of TNF and type I IFNs abrogated the recruitment of mCherry$^+$DCs to the TdLN after VSV$^{\Delta M51}$ treatment (Fig. 6d), and reduced surface expression of CD80 and CD86 (Fig. 6e, f).

We next asked whether serum factors produced by non-cancer cell infections influence the ability of DCs to cross-present antigen. To explore this, we employed the murine cDC1 cell line, MuTuDC1940 (referred to as MuTuDCs)[50], which is frequently used as a model system for antigen cross-presentation. Interestingly, treatment of MuTuDCs with VSV$^{\Delta M51}$-conditioned serum (pooled from mice infected 6 or 12 hours earlier with VSV$^{\Delta M51}$) led to increased presentation of soluble, full-length OVA protein to CD8$^+$ T cells, an effect that was mediated entirely by type I IFNs (Fig. 6g). Notably, direct presentation of SIINFEKL peptide, which is loaded exogenously into MHC I[51], was also upregulated with VSV$^{\Delta M51}$-conditioned serum (Fig. 6h), likely due to cytokine-induced upregulation of MHC I. Thus, to determine whether upregulation of MHC I accounted for the increased presentation of soluble OVA, or whether VSV$^{\Delta M51}$-conditioned serum enhanced bona fide antigen cross-presentation, we studied the cross-presentation pathway upstream of MHC I antigen presentation. We found that VSV$^{\Delta M51}$-conditioned serum induced the formation of galectin-3 (Gal3) puncta around endosome-like structures (Fig. 6i), which is associated with enhanced endosome-to-cytosol escape of antigen, and increased cross-presentation[51,52]. Thus, inflammatory factors produced by VSV$^{\Delta M51}$ infected non-cancer cells not only enhance DC activation and migration to the dLN, but also their ability to cross-present antigen.

Finally, we aimed to determine the importance of these factors in antitumour T cell activation. Consistent with their role in promoting DC function, neutralizing both TNF and type I IFNs abrogated OT-I cell proliferation in M3-9-M$^{Res1/OVA}$ TdLNs after VSV$^{\Delta M51}$ treatment (Fig. 6j). Further, if either type I IFNs alone or in combination with TNF were neutralized, VSV$^{\Delta M51}$ treatment no longer generated tumour regression (Fig. 6k). However, delivery of physiologically relevant doses[53–56] of these cytokines alone was ineffective at inducing tumour regression

https://doi.org/10.1038/s41467-024-54111-6

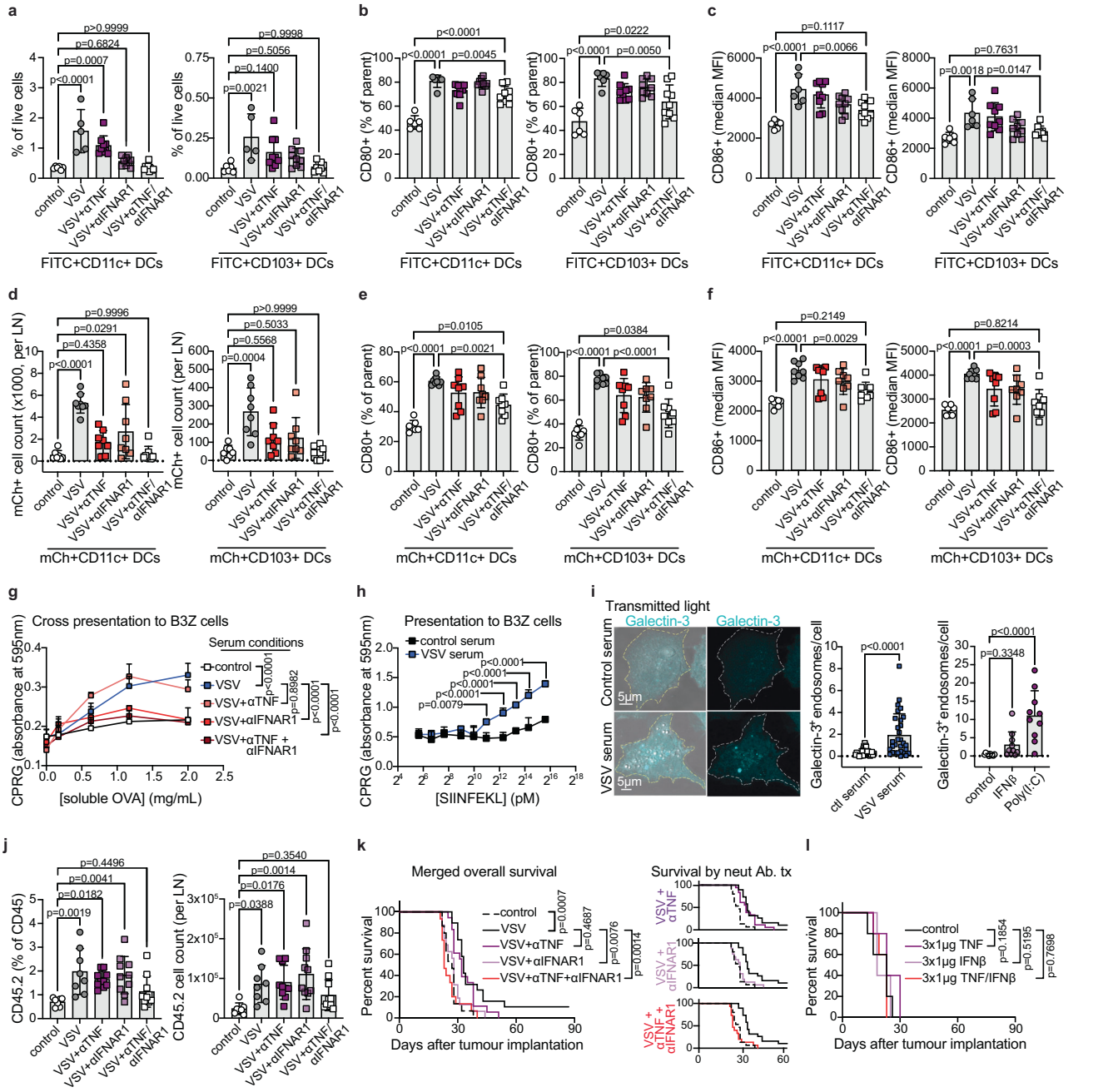

Fig. 6 | Serum factors produced by non-cancer cell infections promote DC migration, activation, and antigen cross-presentation. a–**c** Frequency (**a**) and expression of CD80 (**b**) and CD86 (**c**) on total FITC$^+$ DCs (left) and FITC$^+$CD103$^+$ DCs (right) in the iLN of FITC painted mice 24 h post VSV$^{\Delta M51}$ ± neutralizing antibodies against TNF (αTNF), IFNAR1 (αIFNAR1), or both ($n = 5$–9 mice/group, compiled from 2 independent experiments, one-way ANOVA with Tukey's post-test). **d**–**f** Count (**d**) and expression of CD80 (**e**) and CD86 (**f**) on mCherry$^+$ total DCs (left) and mCherry$^+$CD103$^+$ DCs (right) in the TdLN of M3-9-M$^{Res1/mCherry}$-bearing mice 24 h post VSV$^{\Delta M51}$ ± αTNF, αIFNAR1, or both ($n = 8$ mice/group except $n = 7$ mice/group (control), compiled from 2 independent experiments, one-way ANOVA with Tukey's post-test). **g**, **h** Assay measuring ability of MuTuDCs to present soluble OVA (**g**) or OVA$_{257\text{-}264}$ peptide (**h**) to B3Z cells after pre-treatment with control or VSV$^{\Delta M51}$-conditioned serum ($n = 3$ wells/condition, representative of 2 (**h**) or 3 (**g**) independent experiments, two-way ANOVA with Sidak's post-test on last data-point). **i** Representative images (left) and quantification (middle, right) of galectin-3 puncta in MuTuDCs treated for 24 h under indicated conditions (middle: $n = 30$ fields of view, compiled from 3 independent experiments, two-tailed, unpaired t test; right: $n = 10$ fields of view, one-way ANOVA with Dunnett's post-test). **j** Frequency (left) and count (right) of OT-I cells in the TdLN of M3-9-M$^{Res1/OVA}$-bearing mice, post OT-I cell transfer and treatment with VSV$^{\Delta M51}$ ± αTNF, αIFNAR1, or both ($n = 7$ mice/group (control), $n = 8$ mice/group (VSV), $n = 10$ mice/group (VSV + αTNF, VSV + αIFNAR1, VSV + αTNF/αIFNAR1), compiled from 2 independent experiments, one-way ANOVA with Dunnett's post-test). **k** (left) Merged overall survival of M3-9-M^{Res1}-bearing mice treated with PBS or VSV$^{\Delta M51}$ ± αTNF, αIFNAR1, or both ($n = 15$ mice/group (control, VSV + αTNF + αIFNAR1), $n = 16$ mice/group (VSV + αIFNAR1), $n = 18$ mice/group (VSV + αTNF), $n = 19$ mice/group (VSV), compiled from 3 independent experiments, log-rank Mantel-Cox test between indicated groups); (right) Graphs depicting same data but with only PBS, VSV$^{\Delta M51}$ and indicated neutralizing antibody group. **l** Overall survival of M3-9-M^{Res1}-bearing mice treated with mTNF, mIFNβ, or both ($n = 5$ mice/group, log-rank Mantel-Cox test between indicated groups). In all experiment, VSV$^{\Delta M51}$ was delivered i.v. at 5×10^8 PFU. Points/bars at mean ± SD. For each subfigure showing data for both CD11c$^+$ cells and CD103$^+$ cells, the same samples were used to measure CD11c and CD103. Source data are provided as a Source Data file. Occasionally n is given as a range as the number of mice in each group varies. Please see the Source Data file for the exact n in each group.

(Fig. 6l), demonstrating that while these factors are necessary for antitumour immune responses generated by VSV$^{\Delta M51}$, they alone are not sufficient to elicit antitumour activity.

Together, these results suggest that systemic production of TNF and type I IFNs after i.v. VSV$^{\Delta M51}$ delivery concurrently promotes DC migration, activation and cross-presentation, resulting in heightened antitumour T cell activation and improved tumour control.

Splenic infections produce IFNs and contribute to tumour regression

In addition to the LNs, the spleen also represents a major reservoir of infection after systemic VSV delivery[28,29] (Fig. 7a, b). We thus hypothesized that splenic infections may contribute to virus-induced systemic cytokines and the subsequent enhancement of DC function. To test this, we performed splenectomy surgeries on mice following virus infusion. Because virus titers post-infusion peak in the spleen at 10 minutes (Fig. 7b), and because most VSV$^{\Delta M51}$-induced cytokines and chemokines are not yet expressed at 30 minutes post-infusion (Supplementary Fig. 9c–e), we carried out either splenectomy or sham surgeries 30 minutes after virus delivery. Importantly, sham surgery did not affect virus titers in the spleen when compared to control mice that did not undergo surgery (Supplementary Fig. 9f).

Interestingly, we found that type I and II IFNs were reduced in the serum following splenectomy, demonstrating that the spleen contributes to production of these cytokines following systemic virus administration (Fig. 7c). However, levels of TNF (Fig. 7c) and other cytokines (Supplementary Fig. 9g) were largely unaffected by splenectomy, indicating that they are produced by other sources. Given the spleen's role in producing IFNs following systemic virus administration, we next investigated the role of splenic infections in promoting DC activation and migration to the LN. In the FITC painting model, we found that VSV$^{\Delta M51}$ enhanced recruitment of FITC^{+}CD103^{+} DCs to the LNs of mice that underwent sham surgery. However, in splenectomized mice, recruitment induced by virus treatment was blunted and no longer statistically significant (Fig. 7d, e). Nonetheless, in all groups, VSV$^{\Delta M51}$ still enhanced surface expression of CD80 and CD86 on DC populations (Fig. 7f), likely due to infections in the LN as well as cytokines produced outside of the spleen.

Finally, we asked whether splenic infections impact the therapeutic response elicited by systemic VSV$^{\Delta M51}$ treatment (Fig. 7g). Unexpectedly, we found that sham surgery significantly attenuated VSV$^{\Delta M51}$-induced tumour regression and overall survival, potentially via the immunosuppressive effects of a wound-healing response[57]. Importantly, however, VSV$^{\Delta M51}$-induced antitumour activity was completely abrogated in splenectomized mice (Fig. 7h). This dependence on the spleen was specific to VSV$^{\Delta M51}$ therapy, as tumours in splenectomized mice still responded equally well to PD-1 blockade as mice that underwent sham surgery (Supplementary Fig. 10).

Collectively, these data suggest that splenic infections contribute to VSV$^{\Delta M51}$-induced tumour regression, likely through the production of type I IFNs that promote DC migration to the TdLN.

Type I IFN and TNF enhance costimulation on cDCs within human tumours

Finally, we sought to determine whether the mechanism by which non-cancer cell infections elicit antitumour immunity in mice may also occur in human patients. It has previously been shown that TNF and type I IFNs (both IFNα and IFNβ) are elevated in the serum of patients following i.v. delivery of oncolytic VSV-IFNβ[8]. Given that these cytokines contribute to upregulation of DC co-stimulatory markers upon VSV$^{\Delta M51}$ treatment (Fig. 6e, f), we asked whether they could similarly enhance cDC activation within patient tumours. We obtained four surgically resected, treatment-naïve, tumour samples from patients with head and neck cancer and exposed them ex vivo to both TNF and IFNβ (Fig. 8a). 24 hours later, we measured expression of MHC class I and the costimulatory markers CD80 and CD86 on total DCs and cDC1s (CD141^{+} DCs) (Supplementary Fig 11). While cytokine treatment did not significantly alter the frequency of DCs among immune cells within the tumour samples (Fig. 8b), it did result in significantly increased expression of CD80, as well as a trend towards increased MHC class I and CD86 (Fig. 8c–e). Thus, it is likely that systemic inflammation following VSV delivery to patients can improve the activation of DCs within the tumour, which may result in enhanced antigen presentation and tumour control.

Discussion

Overall, this work describes contributions of both cancer and non-cancer cell infections to antitumour immunity after i.v. VSV$^{\Delta M51}$ delivery. Through the development of cancer cell lines that lack VSV$^{\Delta M51}$ entry receptors, we show that even in the absence of measurable cancer cell infection, systemically delivered VSV$^{\Delta M51}$ can elicit tumour regression and durable cures. This occurs through the infection of non-cancer cells and subsequent production of inflammatory cytokines, such as type I IFNs and TNF, which promote DC migration, activation, and antigen presentation to antitumour T cells in the TdLN. Similarly, DCs in human head and neck cancers upregulate activation markers upon ex vivo treatment with type I IFNs and TNF, suggesting that human DCs in patient tumours can be activated by virus-induced cytokines. This is congruent with previous reports highlighting the importance of these cytokines in DC activity[48,49].

Our results are consistent with recent findings suggesting that productive infection of cancer cells is not always required for OVs to elicit tumour regression. Indeed, for several OVs, including HSV[20], NDV[58], and reovirus[18], it has been shown that cancer cell lines that are relatively resistant to infection in vitro still regress after virus treatment in vivo. Similarly, studies have demonstrated that the efficacy of OV therapy can remain unhindered even when tumour infection is reduced in vivo—either through pre-immunization of mice with OVs[19], the use of single-cycle, replication-incompetent viruses[17], or the use of tumour lines that support little virus infection[16]. It is thus conceivable that other OV platforms may induce tumour regression in the absence of measurable cancer cell infection, similar to what we observed with VSV$^{\Delta M51}$.

Our data suggest that in infection-resistant tumour models, OVs may broadly act as immune adjuvants, by potentiating immune responses at sites of inflammation. Supporting this, it has been shown that VSV$^{\Delta M51}$ elicits innate immune activation through multiple redundant pathways, including through MyD88, toll-like receptor 4 (TLR4), TLR-7 and IL-1[59]. Given its ability to activate several pathogen recognition receptors (PRR), along with its replication and persistence in SLOs, VSV$^{\Delta M51}$ may stimulate pre-existing immunity more potently than other synthetic adjuvants. Further, our results demonstrate that VSV$^{\Delta M51}$ treatment is more effective than discrete delivery of TNF and IFNβ, either because viral persistence allows continuous production of cytokines that otherwise have short half-lives[60–62], or because other virus-induced factors are needed in concert with TNF and IFNβ.

This adjuvant activity could explain why VSV$^{\Delta M51}$ enhanced DC recruitment to the dLN not only in the tumour setting, but also in the FITC painting model, in which inflammation was locally induced during the application of FITC. Further, it is congruent with our finding that among infection-resistant tumour models, only those that were immunogenic responded to VSV$^{\Delta M51}$ treatment. This has similarly been observed with other OVs, including HSV[20,34]. It is therefore possible that clinical responses to OVs may be predicted by tumour immunogenicity, although this requires further study. In particular, it would be interesting to determine whether there is a correlation between treatment response and tumour immunogenicity in settings where tumours are refractory to infection, such as in the phase I clinical trial testing single dose, i.v.-administered VSV in patients with hematological malignancies[8]. VSV was shown to induce both type I IFNs and TNF

https://doi.org/10.1038/s41467-024-54111-6

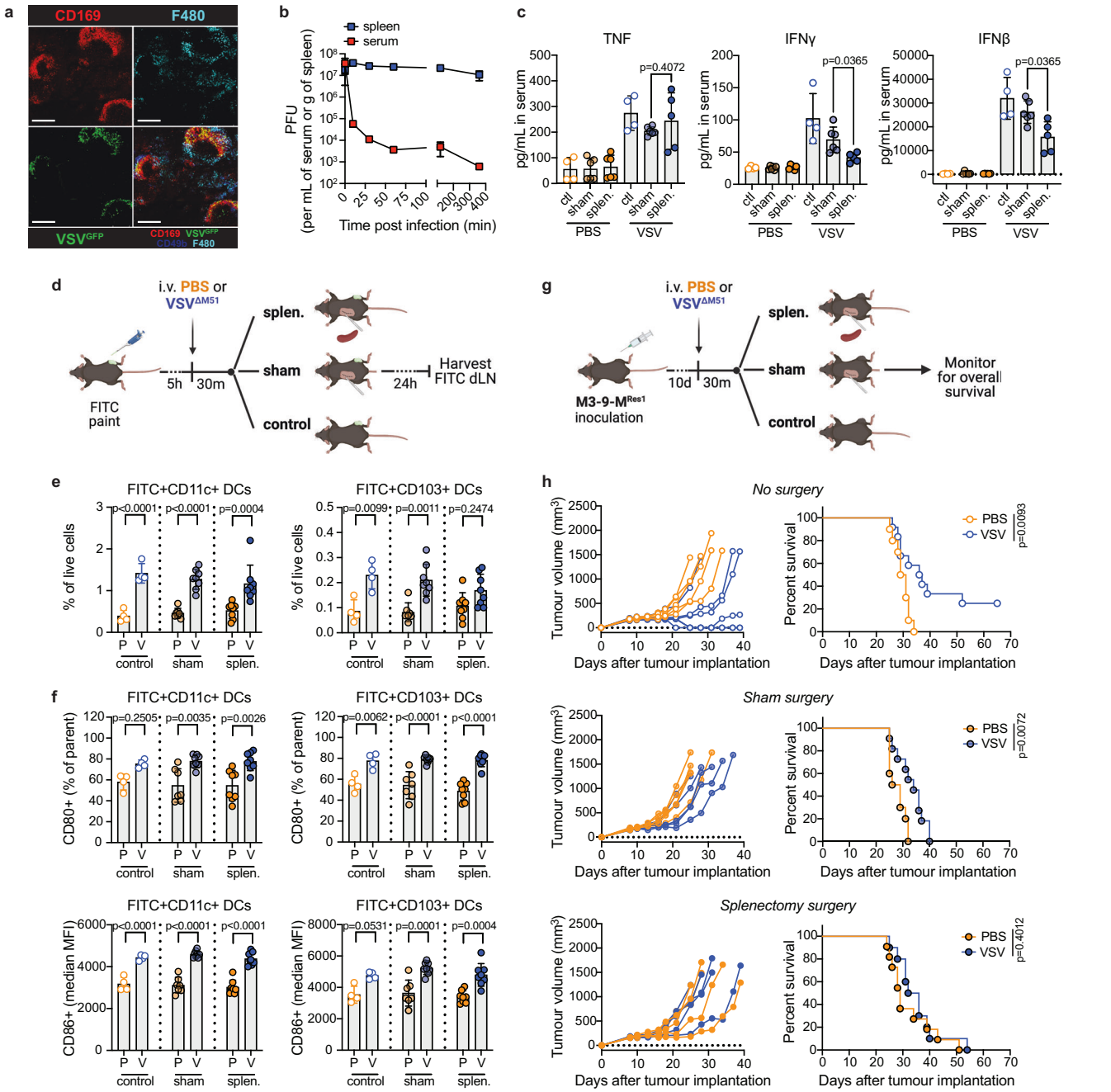

Fig. 7 | Splenic infections produce type I IFNs and contribute to VSV$^{\Delta M51}$-induced antitumour immunity. a Ex vivo image of spleen 6 h post VSV$^{\Delta M51\text{-}GFP}$, representative of $n = 6$ mice imaged over 2 independent experiments. Scale bars are 200 μm. **b** Virus titers in spleen or serum at indicated time points post VSV$^{\Delta M51\text{-}GFP}$ ($n = 3$ mice/group.) **c** Levels of TNF and IFNs in serum 6 h after mice received PBS or VSV$^{\Delta M51\text{-}GFP}$, followed by sham or splenectomy surgery ($n = 4$ mice/group (ctl PBS, ctl VSV), $n = 5$ mice/group (splen. VSV), $n = 6$ mice/group (sham PBS, sham VSV, splen. PBS), compiled from 2 independent experiments, multiple two-tailed, unpaired t tests between sham VSV and splen. VSV groups, with Holm-Sidak post-test). **d** Schematic of FITC painting technique with PBS (P) or VSV$^{\Delta M51}$ (V) treatment followed by sham or splenectomy surgeries. **e**, **f** Frequency (**e**) or expression of CD80 and CD86 (**f**) on FITC$^+$ DCs (left) and FITC$^+$CD103$^+$ DCs (right) in the iLN of mice treated as in **d** ($n = 4$ mice/group (control P, control V), $n = 7$ mice/group (sham P), $n = 8$ mice/group (sham V, splen. P, splen. V), where the same samples were used to measure both FITC$^+$CD11c$^+$ DCs and FITC$^+$CD103$^+$ DCs, compiled from 2 independent experiments, one-way ANOVA with Tukey's post-test). **g** Schematic to determine the contribution of splenic infections to tumour regression. **h** Tumour growth (left) and overall survival (right) of M3-9-M^{Res1}-bearing mice treated with PBS or VSV$^{\Delta M51}$, followed by no surgery (top), sham surgery (middle) or splenectomy surgery (bottom) (left: $n = 5$ mice/group except $n = 6$ mice/group (no surgery VSV), representative of 2 independent experiments; right: $n = 10$ mice/group (no surgery PBS, sham surgery PBS, splenectomy surgery PBS, splenectomy surgery VSV), $n = 11$ mice/group (sham surgery VSV), $n = 12$ mice/group (no surgery VSV), compiled from 2 independent experiments, log-rank Mantel-Cox test). In all experiment, VSV$^{\Delta M51}$ was delivered i.v. at 5×10^8 PFU. Points/bars at mean ± SD. Schematics in **d** and **g** were created in BioRender. Lab, M (2024) BioRender.com/m62j741. Source data are provided as a Source Data file. Occasionally n is given as a range as the number of mice in each group varies. Please see the Source Data file for the exact n in each group.

https://doi.org/10.1038/s41467-024-54111-6

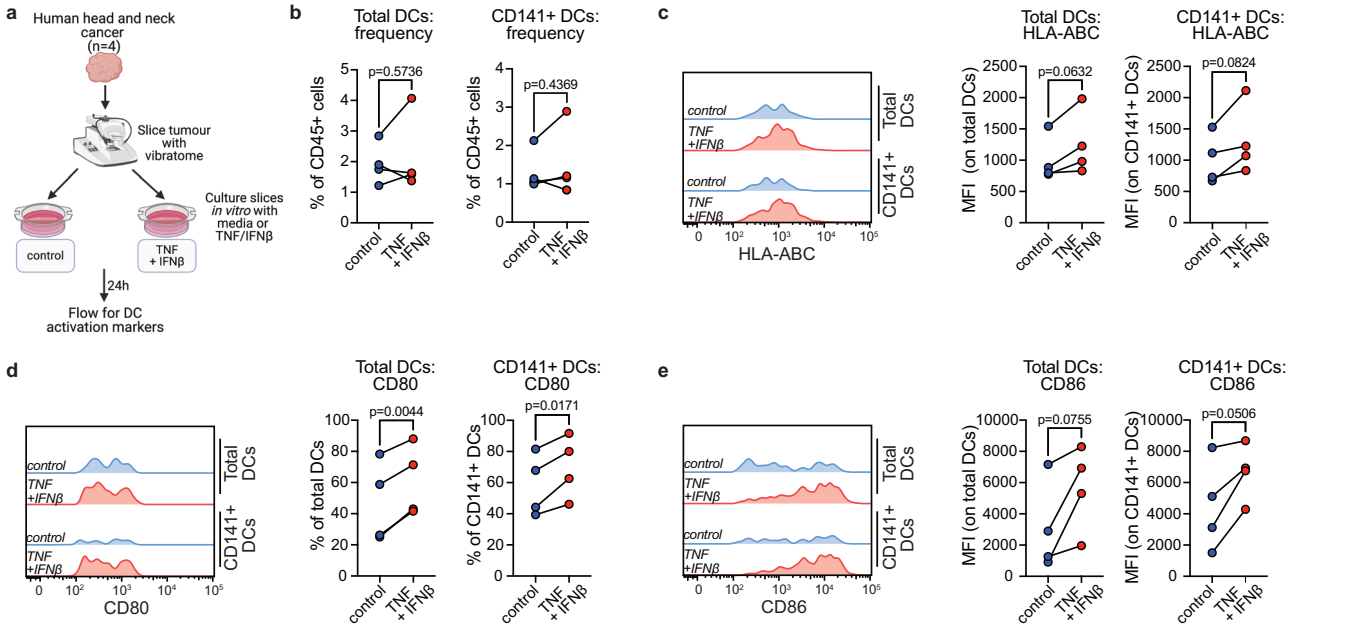

Fig. 8 | Type I IFN and TNF induce costimulatory marker expression on DCs in human tumours. a Schematic of experiment using human head and neck tumour samples. **b** Frequency of total DCs (left) and CD141$^+$ DCs (right) in human tumors treated for 24 h ex vivo with media or hTNF/hIFNβ (20 ng/mL hTNF and 50 ng/mL hIFNβ) ($n = 4$ patient tumours per condition, compiled from 4 independent experiments, two-tailed, paired t test). **c**–**e** Expression of HLA-ABC (**c**), CD80 (**d**) and CD86 (**e**) on total DCs and CD141$^+$ DCs 24 h post treatment with media or hTNF/hIFNβ ($n = 4$ patient tumours per condition, compiled from 4 independent experiments, two-tailed, paired t test). For each treatment condition, the same four samples were used to measure frequency of DCs and expression of HLA-ABC, CD80 and CD86. Schematic in **a** was created in BioRender. Lab, M (2024) BioRender.com/m62j741. Source data are provided as a Source Data file.

in these patients, making it plausible that virus administration potentiates antitumour immunity against immunogenic tumours, similar to what was observed in this study.

Although we did not identify all the non-cancer cell infections that drive therapeutic response in these models, our results suggest that VSV$^{\Delta M51}$ infection in the spleen contributes to systemic IFN production and contributes to virus-induced tumour regression. It is likely that infected splenic cells include CD169$^+$ macrophages and plasmacytoid DCs (pDC), given their susceptibility to VSV$^{\Delta M51}$, and ability to produce type I IFNs[27,46,63]. However, other cell types may also be involved. Intriguingly, other OVs have been reported to either infect or be taken up by the spleen, including vaccinia virus[64], measles virus[24], Maraba[25], and reovirus[23]. It may therefore be possible that the mechanism described for VSV$^{\Delta M51}$ in this study is common to multiple OV platforms.

In addition to exploring the role of non-cancer cell infections in VSV$^{\Delta M51}$ therapy, our study also aimed to better define the mechanisms by which cancer cell infections contribute to antitumour activity. We found that mice bearing immunogenic tumours that were infection-hypersensitive consistently achieved greater cure rates than mice bearing isogenic infection-resistant tumours. This is consistent with previous studies demonstrating that increasing VSV$^{\Delta M51}$ infection of cancer cells using infection sensitizers results in improved tumour regression[65,66]. Interestingly, durable cures in our models still required CD8$^+$ T cells, although even in their absence, significant tumour regression could be achieved by infection within the tumour, likely through cancer cell lysis and debulking of the tumour. Further, we found that VSV$^{\Delta M51}$ infection of cancer cells themselves could induce antitumour activity at an abscopal site. These data are in line with ICD being one mechanism of OV activity, although we did not directly measure ICD in our study. Finally, our data from the infection-hypersensitive model suggest that cancer cell infection may increase tumour immunogenicity. Indeed, while VSV$^{\Delta M51}$ is unable to generate cures in weakly immunogenic tumours in the absence of cancer cell infection, it elicits robust CD8$^+$ T cell-mediated tumour regression in the presence of cancer cell infection. It is possible that virus-induced cell death exposes new tumour antigens against which antitumour immunity is initiated, further supporting the mechanism of ICD.

Taken together, these data imply that infection of both cancer and non-cancer cells plays an important role in driving anticancer immunity after VSV$^{\Delta M51}$ treatment. An interesting avenue for future exploration would be to determine the relative contribution of cancer or non-cancer cell infections to treatment outcome. While our study attempted to isolate the role of non-cancer cell infections in antitumour immunity, we did not study the contribution of only cancer cell infections. This would require a method to deliver virus to the TME while preventing leakage of virions to systemic sites.

One limitation of our work is that we primarily focused on the role of non-cancer cell infections that were distal to the tumour, such as those in the TdLN, or spleen. However, we did not consider the contributions of non-cancer cells in the TME that have been reported to be infected by VSV$^{\Delta M51}$, such as endothelial cells[22]. Although we did not focus on those infections, it is possible that they produce local factors that contribute to antitumour immunity. Further, all tumour models in this study were generated using cancer cell lines. This was essential for our study, as we genetically engineered infection-modulated clonal cell lines. Nonetheless, transplanted tumour models do not faithfully recapitulate the heterogeneity and slower growth kinetics of human tumours. One way to mitigate these concerns in the future is by performing experiments using spontaneous, or induced, tumour models.

Despite these limitations, the results presented herein suggest that systemically delivered VSV$^{\Delta M51}$ induces tumour regression by enhancing antigen presentation, and thus may synergize with other immunotherapies—such as PD-1 blockade—via this mechanism. Although the combination of OVs and immune checkpoint inhibitors has been explored extensively and shown promising clinical activity (reviewed elsewhere[67]), our data suggest that these therapies may partially converge within the TdLN. These mechanistic insights into VSV$^{\Delta M51}$ activity pave the way for other combination therapies to be more rationally designed. For example, given that systemic VSV$^{\Delta M51}$

increases antigen presentation in the TdLN, it may combine well with local treatments that increase the quality of antigen presentation within the tumour, including anthracyclines, or other known ICD-inducers[68]. Further, given the ability of OVs to carry genetic payloads, VSV$^{\Delta M51}$ platforms could be developed to encode payloads that better potentiate their antitumour effects. One possibility is a VSV$^{\Delta M51}$ engineered to encode Flt3L, to promote hematopoietic progenitor commitment to the DC lineage, including to cross-presenting cDC1s. This strategy has improved efficacy of several OVs, including HSV[69] and NDV[70], and may enhance the ability of systemic VSV$^{\Delta M51}$ to improve antigen presentation.

Together, our results generate insight into the complex and coordinated interactions between VSV$^{\Delta M51}$-infected cancer and non-cancer cells, and the induction of antitumour immunity (Supplementary Fig. 12). In addition to elucidating the mechanism of VSV$^{\Delta M51}$-induced tumour regression, our work also generates support for i.v. administration of oncolytic viruses. While this has often been avoided to prevent neutralization, opsonization, or dilution of the virus in the blood, it is possible that i.v. delivery may take better advantage of non-cancer cell infections that contribute to therapeutic response. Overall, these results lay the foundation for the development of more effective virus-based therapies for cancer treatment.

Methods

Mice

BALB/c (H-2d, strain code 028), C57BL/6 (H-2b, strain code 027) and CD45.1 (B6-Ly5.1/Cr, strain code 564) mice were obtained from the Charles River Laboratory Inc. (Montreal, Canada). OT-I (C57BL/6-Tg(TcraTcrb)1100Mjb/J, strain code 003831), Batf3$^{-/-}$ (B6.129S(C)-*Batf3*^{tm1kmm}/J, strain code 013755) and TdTomato reporter (B6.Cg-*Gt(ROSA)26Sor*$^{tm14(CAG-tdTomato)Hze}$/J, strain code 007914) mice were obtained from The Jackson Laboratory Inc. (Bar Harbor, United States). All mice were housed in a biohazard level 2 biocontainment facility at the University of Calgary under a 12 h:12 h light:dark cycle at 20–24 °C and 30–50% humidity, and under specific pathogen-free conditions. At the time of experiment initiation, all mice were approximately 6–8 weeks old and littermates of the same sex were randomly assigned to experimental groups. In most cases, experiments were conducted in female mice due to the immunogenicity of male-derived M3-9-M tumours in female mice. Where indicated, experiments were conducted in male mice. These experiments either involved implanting M3-9-M tumours as a model of low tumour immunogenicity, or M3-9-M^{OVA} cells to control for sex differences in the response of immunogenic tumours to cancer immunotherapy. Animal experiments were approved by the University of Calgary Health Sciences Animal Care Committee (under protocol AC19-0076) and complied with all ethical regulations.

Cell lines

EMT-6 (CRL2755), CT-26^{CL25} (CRL 2639) and Vero (CCL-81) cells were purchased from the American Type Culture Collection (Manassas, VA, USA). CT-26^{IFNmut} cells[31] were received from Dr. John Bell (Ottawa, ON, Canada). M3-9-M[36] and 76–9 cells[71] were obtained from Dr. Crystal MacKall (Stanford, CA, USA). TAO1[37] were received from Dr. Michael Monument (Calgary, AB, Canada). Finally, MuTuDC1940 cells[50] and the B3Z hybridoma line[72] were received from Dr. Johnathan Canton (Calgary, AB, Canada). CT-26^{CL25}, CT-26^{IFNmut}, 76–9, M3-9-M, TAO1 and B3Z cells were propagated in RPMI 1640 (ThermoFisher, 11875093) supplemented with 10% heat-inactivated fetal bovine serum (ThermoFisher, 16140071) and 50 μM β-mercaptoethanol (ThermoFisher, 31350010). EMT-6 cells were cultured in Waymouth's medium (ThermoFisher, 11220035) supplemented with 15% FBS. Vero cells were cultured in DMEM (ThermoFisher, 11965118) supplemented with 10% FBS. MuTuDC1940 cells were cultured in Iscove's Modified Dulbecco's Medium (IMDM, Cytiva, SH30259.02) supplemented with 10% FBS (Corning, 35-087-CV), 100 units/mL penicillin and 100 μg/mL streptomycin (Cytiva, SV30010), 10 mM HEPES (Cytiva, SH30237.01), 0.075% Sodium bicarbonate (Lonza, 17-613E), 1X GlutaMAX (Gibco, 35050-061) and 500 μM 2-mercaptoethanol (Gibco, 31350-010). Aside from MuTu1940s, antibiotics were not added to media used for culturing cells and all lines routinely tested negative for mycoplasma.

Viruses

VSV$^{\Delta M51\text{-}GFP}$ and VSV$^{\Delta M51\text{-}oFluc}$ (both Indiana strains)[73] were obtained from Dr. David Stojdl (CHEO Research Institute). To generate VSV$^{\Delta M51\text{-}creGFP}$, the Cre-2A-GFP insert was first PCR amplified from the TOPO Cre-2A-GFP plasmid (Addgene, 68450) using the primers Cre F and Cre R (Supplementary Table 1) and inserted into the VSV$^{\Delta M51\text{-}GFP}$ vector using restriction enzymes XhoI and NheI (resulting in the plasmid, pVSV$^{\Delta M51\text{-}creGFP}$). To rescue infectious virions, LentiX 293 T cells were infected with 3MOI of vaccinia virus encoding the T7 RNA polymerase. Cells were then transfected with plasmids encoding VSV N, P, L and pVSV$^{\Delta M51\text{-}creGFP}$. Rescued virus was collected 72 h post-transfection, clarified (10 min at 3000 g), and filtered twice through a 0.22 μm filter. Virus was triple plaque purified on Vero cells and clones were verified by next-generation sequencing to ensure they did not contain erroneous mutations with greater than 10% read frequency.

To grow VSV$^{\Delta M51}$, Vero cells were seeded in 145 cm^2 (15 cm) dishes and allowed to reach confluence. Cells were then infected with 0.02MOI of virus in 7 mL of culture media (DMEM + 10% FBS). Plates were incubated for 60 min with agitation every 10 min before 13 mL of culture media was added to each plate. Plates were incubated for 24 h after infection before the infected culture media was collected and clarified by centrifugation at 3000 × *g* for 15 min. The virus-containing supernatant was subsequently pelleted at 18,600 × *g* for 3 h with the J-Lite JLA-10.500 Fixed-Angle Rotor (Beckman Coulter) and allowed to stop with minimal deceleration. The viral pellet was resuspended in 1 mL Phosphate-Buffered Saline (PBS, ThermoFisher, 10010049) before being added to the top of a 10–35% OptiPrep gradient. The gradient was centrifuged at 221,633 × *g* for 95 min with the SW-41 Rotor (Beckman Coulter) and allowed to stop with minimal deceleration. The white gradient band of purified virus was removed and aliquoted into 50 μL increments before freezing at −80 °C. Vaccinia$^{\Delta F4L/\Delta J2R\text{-}mCherry}$ [74] was a kind gift from Dr. David Evans (University of Alberta).

Generation of knockout cell lines using Crispr/Cas9

Generation of CRISPR knockout cell lines was carried out by transfecting cells with target-specific CRISPR RNA (crRNA) and transactivating RNA (tracrRNA) (Dharmacon reagents, Horizon Discovery) along with Cas9 nuclease (Cas9-NLS, Sigma-Aldrich) as a ribonucleoprotein (RNP) complex. In all cases the tracrRNA used was Dharmacon Edit-R CRISPR-Cas9 synthetic tracrRNA (cat no: U-002000-120). crRNAs (Horizon Discovery) used for gene knockouts are listed in Supplementary Table 1. *Ldlr* and *Lrpap1* were targeted simultaneously either in CT-26^{IFNmut} or M3-9-M, whereas *Ifnar1* was targeted alone in M3-9-M only. To generate knockouts, cell lines were seeded in a 6-well plate at a density of 3×10^6 cells/well. The next day, tracrRNA and the appropriate crRNAs were diluted in RNase free water to achieve a concentration of 2 μM of each component. In cases where multiple crRNAs were being used to target the gene of interest, the total concentration of all crRNAs in solution was 2 μM. Similarly, the Cas9 protein was diluted in OPTIMEM media to achieve a concentration of 2 μM. Next, a 660 nm RNP solution was prepared by combining 33.3 μL of OPTIMEM, 33.3 μL of the diluted tracrRNA:crRNA solution, and 33.3 μL of the diluted Cas9 protein. This was mixed and incubated at room temperature (RT) for 10 min. During this time, 7.5 μL of Lipofectamine RNAiMAX transfection reagent (ThermoFisher, 13778075) was added to 100 μL of OPTIMEM. After the 10 min incubation, the RNP solution was mixed with the diluted RNAiMAX and incubated for an additional 10 min before the solution was added dropwise to the cells. The next

morning, media on the cells was changed. Three or four days later, transfected cells were sorted to place a single cell per well of a 96-well plate, to generate clonal populations of cells. Knockout clones were initially identified based on resistance (for *Ldlr/Lrpap1* knockouts) or hypersensitivity (for *Ifnar1* knockouts) to VSV$^{\Delta M51}$ infection.

Genomic DNA isolation and TIDE analysis

Genomic DNA was isolated from cell lines using the geneJET DNA purification kit (ThermoFisher, K0721) according to manufacturer's instructions. Eluted DNA was then PCR amplified around the edit sites. For *Lrpap1*, targeted sites were in exon 2 and were amplified using forward TCTAGCTGGGCTCCTGACAT and reverse AGTTGGTGGC-CAGTCTATGG. For *Ldlr*, targeted sites were either in exon 4 or exon 7. Exon 4 site was amplified using forward GGCAGAAAAGGGTGTGTTGT and reverse GCCATCATATCCAGCCCTTA. Exon 7 site was amplified using forward GCCCCAACAAGTTCAAGTGT and reverse CCTCGATTCGTGATGAGGAT. Primer sequences can also be found in Supplementary Table 1. PCR amplicons were then sent for Sanger Sequencing at the University of Calgary. Sequence chromatograms were uploaded into the TIDE (Tracking of Indels by Decomposition) analysis software (https://tide.nki.nl/) to determine the percentage of alleles that are edited at a given locus.

Western blots

Cell lysates were harvested from confluent 56.7 cm^2 (10 cm) plates and collected in total lysis buffer (50 mM Tris-HCl (pH 8.0), 150 mM NaCl, 1% Triton X-100, and 1% SDS). Samples were then boiled at 95 °C for 5 min, vortexed, and boiled again (95 °C, 5 min). Protein quantitation was performed using the DC Protein Assay Kit II (Bio-Rad, 5000112) as per manufacturer's instructions. The protein concentration of each sample was equalized with the addition of lysis buffer. Subsequently, 5X Laemmli buffer (250 mM Tris-HCl (pH 6.8), 10% SDS, 30% glycerol, 5% β-ME, 0.02% bromophenol blue) was added to each sample, and lysates were boiled again at 95 °C for 5 min. 15 μg of each sample was then resolved through either an 8% SDS-PAGE gel (for detection of LDLR) or a 10% SDS-PAGE gel (for detection of LRPAP1). Proteins were then transferred onto a nitrocellulose membrane using the Trans-Blot Turbo Transfer System (Bio-Rad, 1704150, 25 V, 1.8Amps, 60 min). Membranes were blocked in 5% skim milk (LRPAP1) or 3% BSA (LDLR) diluted in TBS-Tween 20 (0.01%) (TBS-T) for 30 min. Membranes were rocked over night at 4 °C in primary antibody diluted in blocking buffer + 0.05% sodium azide (1:500 of goat anti-mouse LDLR affinity purified polyclonal Ab, R&D systems, #AF2255; 1:1000 of rabbit anti-LRPAP1 antibody, Sigma-Aldrich, #HPA008001). 0.025 μg/mL rabbit anti-α tubulin polyclonal antibody (Abcam, #ab18251) was used as a loading control. The following day, membranes were washed with TBS-T three times, and then incubated in secondary antibodies diluted in blocking buffer for 1 h at RT (for LDLR, 1:1000 donkey anti-goat IgG HRP-conjugated antibody, R&D systems, #HAF109; for LRPAP1, 1:2000 Peroxidase AffiniPure goat anti-rabbit IgG (H + L), Jackson Labs, #111-035-003). Membranes were again washed with TBS-T three times and immunoreactive proteins were detected using the Clarity™ Western ECL Substrate (Bio-Rad, 1705060) on a Chemidoc-IT Imager (UVP, Upland, CA, USA).

Mouse tumour models

Tumour cells were harvested by trypsinization and washed twice with PBS. For M3-9-M, 76-9 and TAO1 tumour models, C57BL/6 mice were inoculated intramuscularly in the lateral gastrocnemius with 5×10^4 cells (for M3-9-M and 76-9) or 1×10^4 cells (for TAO1) in 50 μL PBS. For most experiments, tumours were only established in one leg, except bilateral hindlimb flank studies, where tumours were implanted into both legs. For CT-26^{IFNmut} and CT-26^{CL25}, Balb/c mice were inoculated subcutaneously under the skin of the hindlimb with 1×10^6 cells in 50 μL PBS. For EMT-6, Balb/c mice were inoculated in the mammary fatpad with 2×10^5 cells in 50 μL PBS. Tumour sizes were measured using digital calipers twice or three times per week. The maximum size of tumours allowed by The University of Calgary Health Sciences Animal Care Committee was 1.7 cm in any direction and we adhered to this limit in all experiments. Without exception, mice were euthanized by CO_2 inhalation or cervical dislocation once tumours reached this size, or were terminated early if ulceration occurred.

Mouse treatment regimens

For experiments involving tumour-bearing mice, tumours were measured using skin calipers before treatment initiation, and mice were randomized so that experimental groups had similar average tumour volumes. For most studies, mice were treated on day 10 with either PBS, VSV$^{\Delta M51}$, or UV-inactivated VSV$^{\Delta M51}$ (5×10^8 PFU, delivered i.v.). Where indicated, VSV$^{\Delta M51}$ was administered subcutaneously to the right lower flank, rather than i.v. For FITC painting experiments, the right hindlimbs of mice were shaved and painted with 50 μL of 2% FITC solution (prepared fresh by dissolving FITC isomer 1 (Sigma-Aldrich, F7250) into a 1:1 solution of acetone and dibutyl phthalate.) For antibody neutralization experiments, mice were injected intraperitoneally (i.p.) with 250 μg of anti-CD8 (clone 2.43; BioXCell) monoclonal antibody on day 7 post tumour implantation, followed by 100 μg on days 10, 14, 21, 28, 35. Efficiency of T-cell depletion was monitored by flow cytometry using the anti-CD8 antibody (diluted 1:100, clone 53–6.7, Biolegend). For PD-1 blockade, mice were typically administered 250 μg anti-PD-1 i.p. (clone RMP1-14, BioXCell) on days 7, 10 and 13. In some experiments, anti-PD-1 was delivered only on day 10, at the indicated doses. For neutralization of TNF or type I IFNs, mice were i.p.-delivered 250 μg of either anti-TNF (clone XT3.11, BioXCell), anti-IFNAR1 (clone MAR1-5A3, BioXCell) or both, 1 h after delivery of VSV$^{\Delta M51}$. For experiments involving in vivo cytokine treatments, mice bearing day 10 tumours were i.p.-delivered 1 μg of either recombinant mouse IFN-β1 (Biolegend, 581306), recombinant mouse TNF (Biolegend, 575206), or both every 6 h for a total of 3 doses. Finally, for studies requiring blockade of lymphocyte egress from the LNs, mice were i.p.-delivered FTY-720 (Sigma-Aldrich, SML0700, 20 μg per mouse) on day 9, 10, and subsequently every 2 or 3 days for the remainder of the study.

In vitro VSV$^{\Delta M51}$ growth kinetics

Cancer cell lines were plated in 6-well plates and allowed to adhere overnight. The next morning, cells were infected with VSV$^{\Delta M51\text{-}GFP}$ at an MOI of 0.01 in an infection volume of 0.3 mL of DMEM. After 60 min of incubation (37 °C and 5% CO2), 1.7 mL of DMEM + 10% FBS were added to wells, and cells were returned to the incubator. Across a 72 h period, 2 mL of virus-containing medium was collected at 12 or 24 h intervals from individual infected wells and frozen at −80 °C prior to titering on Vero cells. When ready for titering, samples were thawed on ice, serially diluted in PBS and plated on Vero cells in 6-well plates. Infected Vero cells were cultured in DMEM medium supplemented with 10% FBS containing 1% carboxymethyl cellulose for 24 h, and then fixed and stained with crystal violet. Where possible, plaque counts were determined from wells containing 30–150 plaques.

Cell viability assays

For viability assays, cells were seeded in 96-well flat bottom plates such that they would reach 50% confluent the next day. For experiments involving IFNAR1 knockout clones, cells were given approximately 8 h to adhere to the plates, and then were pre-treated with 250 pg/mL mouse IFN-β for 12 h. The next morning, serial dilutions of VSV$^{\Delta M51\text{-}GFP}$ were prepared in complete RPMI and cells were infected with a range of MOIs (spanning 0.001 to 100MOI). For studies involving Vaccinia$^{\Delta F4L/\Delta J2R}$, cells were instead infected with Vaccinia$^{\Delta F4L/\Delta J2R}$ at MOIs of 10, 3, 1 and 0.3. Plates were then incubated with virus at 37 °C + 5% CO2. 48 to 72 h later, media was removed from cells and replaced with 100 μL of

1xalamarBlue Cell Viability Reagent (ThermoFisher, DAL1100) diluted in RPMI. Plates were again incubated at 37 °C + 5% CO2 for 3-4 h (or until media started to become pink). Finally, the fluorescent signal from each well was read with a fluorescent plate reader (excitation/emission−560/590 nm). Data is represented as the percent of live cells in virus treated conditions compared to control (untreated) conditions.

Generation and validation of M3-9-M with cre-inducible mCherry

To generate the plasmid for constitutive mTagBFP2 expression and cre-inducible mCherry expression, an mTagBFP2 gene was PCR amplified from the mTagBFP2-pBAD plasmid (Addgene, 54572) and cloned upstream of a T2A sequence in a lentivirus expression vector (pLV-eGFP, Addgene, 36083), modified to be driven by the Murine Stem Cell Virus (MSCV) promoter. Next, a loxP-STOP-loxP sequence (PCR amplified from the pCAG-loxPSTOPloxP-ZsGreen plasmid, Addgene, 51269) was cloned downstream of the T2A, followed by the gene encoding mCherry.

To produce lentivirus, MDLg/pRRE (Addgene, 12251), pRSV-Rev (Addgene, 12253), pCL-Eco (Addgene, 12371) and the MSCV-mTagBFP2-LSL-mCh plasmid were transfected into LentiX cells with Lipofectamine 2000 (ThermoFisher, 11668019) at a ratio of 5:2:1:5, respectively. 48 h and 72 h post transfection, media containing lentivirus was collected and combined, filtered through a 0.45 μm filter and concentrated 10x using a 100 kDa Amicon Ultra-15 Centrifugal Filter Unit (Millipore, UFC9100). To transduce M3-9-M, tumour cells were harvested and resuspended to 4×10^5 cells/mL. Concentrated lentivirus was then diluted by mixing 100 μL of virus with 150 μL RPMI, and polybrene (Sigma-Aldrich, TR-1003) was added to a final concentration of 16 μg/mL. 250 μL of this solution was then added to 250 μL of resuspended M3-9-M cells, plated in one well of a 24-well plate, and centrifuged at 931 × *g* for 2 h at 30 °C. After centrifugation, cells were topped with 1 mL of complete RPMI, and incubated overnight. Cell lines were then flow sorted twice on mTagBFP2 to obtain a transduced population (M3-9-$M^{BFP2\text{-}LSL\text{-}mCh}$).

To validate the cell line, M3-9-$M^{BFP2\text{-}LSL\text{-}mCh}$ cells were plated in a 24-well plate at 1×10^5 cells/well and allowed to adhere overnight. The next day, cells were infected with 1, 5 or 10MOI of $VSV^{\Delta M51\text{-}creGFP}$ in serum free RPMI and incubated for 1 h at 37 °C, followed by removal of $VSV^{\Delta M51\text{-}creGFP}$-containing media and replacement with complete RPMI containing 2.5 ng/mL recombinant mouse IFNβ (R&D systems, 8234-MB-010). Flow cytometry on cell lines was then carried out at 6 and 96 h post infection to measure GFP and mCherry expression on $mTagBFP2^+$ cells.

In vitro antigen presentation assays

For cross presentation assays using soluble OVA, 5×10^4 MuTuDCs were seeded in a round bottom 96-well plate and incubated overnight at 37 °C with 5% CO2 (day 1). The next day (day 2), media on MuTuDCs was removed and replaced with 100 μL of control mouse serum or $VSV^{\Delta M51}$ conditioned mouse serum (see *serum transfers*) that was diluted to 25% in complete IMDM media. In some experiments, MuTuDCs were first incubated with 25 μg/mL anti-TNF, 20 μg/mL anti-IFNAR1, or both for 1 h at 37 °C, and diluted serum was incubated with the same concentrations of neutralizing antibodies for 1 h at 4 °C. Subsequently, media on MuTuDCs was removed and replaced with 100 μL of serum containing neutralizing antibodies. Endotoxin-free OVA (Sigma-Aldrich, A5503) was then diluted in PBS and added to wells of MuTuDCs to achieve concentrations indicated in the results. Cells were incubated with serum and soluble antigen overnight. The next day (day 3), media was removed, and 1×10^5 B3Z hybridoma cells were added per well. After 20–24 h (day 4), cells were pelleted by spinning plates at 300 × g for 5 min at RT, washed once in PBS, and then incubated with lysis buffer containing 9 mM $MgCl_2$, 0.125% NP40 (Nonidet P40 substitute, Sigma-Aldrich, 74385), and 1.5 mM chlorophenol red-β-D-galactopyranoside (CPRG, GoldBio, 99792-50-4). Lysis was allowed to proceed for 2–4 h at 37 °C. CPRG conversion by β-galactosidase was measured by optical density at 595 nm. For experiments involving presentation of SIINFEKL peptide ($OVA_{257\text{-}264}$), the procedure was similar to above, except instead of adding soluble OVA on day 2, SIINFEKL peptide (Sigma-Aldrich S7951) was added on day 3. Peptide was first diluted in complete IMDM media at indicated concentrations. Media from MuTuDCs was then removed and replaced with SIINFEKL containing media, and cells were incubated at 37 °C for 2 h. Cells were then washed twice with serum free IMDM media to remove unbound SIINFEKL peptide, and 1×10^5 B3Z cells were added as above. B3Z activation was measured by CPRG conversion, as described above.

Galectin-3 immunofluorescence staining

1×10^5 MuTuDCs were plated in complete IMDM onto an 8-well chambered slide (ibidi, 80826) and allowed to adhere overnight. The next day, media on MuTuDCs was removed and replaced with either 200 μL of complete media, mIFNβ (2 ng/mL), poly:IC (1:1000, InvivoGen, tlrl-pic), control mouse serum (diluted to 25% in complete IMDM media), or $VSV^{\Delta M51}$ conditioned mouse serum (diluted to 25% in complete IMDM media). Cells were incubated with treatments overnight. The next morning, media was removed from the plate, and cells were challenged with 20 μg/mL ovalbumin-Alexa Fluor 488 (ThermoFisher, O34781) for 3 h. After this time, cells were fixed with 4% paraformaldehyde (PFA, Electron Microscopy Sciences, 15710) in PBS for 20 min at RT and quenched with 3 washes of 50 mM ammonium chloride (Sigma, A0171) in PBS. Cells were washed 3 times with fresh PBS and permeabilized using 0.1% Triton X-100 (Sigma, X100) in PBS for 15 min at RT. After 3 washes with fresh PBS, cells were blocked with 2% non-fat powdered milk in PBS (blocking buffer) for 15 min, and subsequently stained with α-Galectin-3 (1 μg/mL in 2% milk in PBS). Cells were then washed 3 times with blocking buffer, 3 times with PBS and imaged on a Leica SP8 18-24 h later.

Ex vivo whole mount imaging of lymph node and spleen

For ex vivo imaging of spleen and lymph nodes, organs were harvested following euthanasia from mice previously treated with $VSV^{\Delta M51}$ and/or with fluorescently labeled antibodies. Lymph nodes were blotted and placed directly onto the microscope cover glass. Spleens, following removal, were placed capsule side down and sectioned lengthwise to expose the follicles. The sectioned side was then blotted and placed cut-side down onto the microscope cover glass. Kimwipes soaked in PBS were placed over the organs to maintain moisture while imaging.

Intravital microscopy

Surgical preparation was completed as previously described[75]. Briefly, mice were anaesthetized with a ketamine and xylazine mixture (200 μg/g and 10 μg/g, respectively; delivered i.p.). A venous catheter was inserted in the tail vein to allow the administration of fluorescent antibodies and maintain the anesthetic. For subcutaneous tumours ($CT\text{-}26^{CL25}$, $CT\text{-}26^{IFNmut}$, EMT-6), the mice were positioned on their abdomens and secured in place with surgical tape. Ethanol and sterile mineral oil were used to saturate the dorsal area to limit fur from entering the surgical and imaging sites. An incision was made from the base of the tail continuing up to the neckline on the side of animals with a tumour. The skin was lifted away from the body, reflected laterally, and the overlying fascia layer was removed. Two sutures were placed along the cut border of the skin flap to allow it to be stretched out and secured to a blank microscope slide. The animals were inverted and placed on their back on a heated microscope stage (37 °C), allowing the skin flap with the tumor to be extended over the imaging window, and the stage was then transferred to the inverted microscope. For intramuscular tumours (M3-9-M, 76-9, TAO1), as with the preparation of subcutaneous tumors, the mouse was anesthetized, and

the tail vein was cannulated. The tumor-bearing leg was extended, and a small incision was made in the skin located directly over the tumor mass. The skin layer was slowly removed, with care taken not to damage any major vessels. PBS was applied to the tumor every 10 min to maintain tissue moisture, and the animal was set in a lateral position on a heated microscope stage so that the tumor was located directly on the cover glass. The leg was gently secured in place with tape, with care taken not to block or restrict the blood flow. The heated stage was transferred to the microscope. IVM was performed using a Leica SP8 inverted microscope (Leica Microsystems, Concord, ON, Canada). Microscopy data was processed and analyzed using Leica Las X software and Fiji: ImageJ.

LN immunofluorescence

Lymph nodes were isolated from mice and fixed in 4% PFA overnight at 4 °C. Fixed tissue were then rinsed once in PBS and placed in 30% sucrose (Sigma-Aldrich, SO389) overnight. The next morning, lymph nodes were embedded in Tissue-Tek O.C.T. (optimal cutting temperature, Sakura Finetek, 4583) compound and frozen on dry ice. Frozen blocks were then sliced using a cryostat to generate 10–20 μm sections. Slides were fixed in acetone at −20 °C for 20 min. The slides were then stored at −20 °C (short-term storage), or −80 °C (long-term storage) until ready for staining. On the day of staining, slides were washed with PBS for 10 min, then blocked with 5% mouse serum (Jackson ImmunoResearch, 015-000-120) for 1-2 h to minimize non-specific binding and background. Slides were then incubated overnight with primary antibodies (1:200 for αGFP and αPNAd; 1:500 for αLYVE-1; 1:100 for αCD169) diluted in 5% mouse serum at 4 °C. On the second day, slides were washed three times with PBS (immersed for 10 min for each wash), and then incubated with secondary antibodies (AffiniPure Donkey anti-Rat IgG (H + L) AF647 or AffiniPure Donkey anti-Rabbit IgG (H + L) Cy3) diluted to 1:200 in 5% mouse serum for 1 h at RT. Finally, samples were washed three times with PBS (10 min immersion in PBS for each wash) and mounted with glass coverslips using VECTASHIELD Antifade Mounting Media with DAPI (Vector Laboratories, H-1200-10).

Flow cytometry

Spleens and lymph nodes were isolated from mice and gently mashed through 70 μm cell strainers to generate single cell suspensions. Splenocytes were then pelleted and subjected to red blood cell lysis using 1x RBC Lysis Buffer (Biolegend, 420301) for 5 min at RT. Both lymph node cells and splenocytes were finally resuspended in cold PBS for staining. Tumours were harvested from mice, weighed, and minced into pieces ~2–4 mm in diameter. Tumour pieces were then placed into a gentleMACs C tube (Miltenyi Biotech) containing 5 mL of digestion buffer (RPMI with 2 mg/mL Collagenase II (Sigma-Aldrich, C6885), 0.05 mg/mL DNase I (Sigma-Aldrich, DN25)). The samples were then homogenized using the gentleMACS protocol m.imp.tumor.01, incubated for 45 min at 37 °C on a shaker, and then homogenized again using the gentleMACS protocol m.imp.tumor.02. Tumour cell suspensions were then strained through a 70 μM filter and pelleted at 350 × *g* for 5 min at 4 °C. Next, red blood cells were lysed by treating cells with 1× RBC lysis buffer (for 5 min at RT). Tumour cells were then pelleted again at 350 × *g* for 5 min and resuspended in isotonic 40% Percoll to separate fat and debris from cells by density centrifugation (400 × *g* for 20 min at RT). Supernatant was then carefully poured off, and pellets were washed once in PBS, followed by resuspension in cold PBS for staining. Blood was collected from mice via cardiac puncture using a 1 mL syringe precoated with 50 μL 0.5 M EDTA. 500 μL of blood was then subjected to two rounds of red blood cell lysis using 1× RBC lysis buffer (5 min at RT each). Blood cells were then resuspended in ice cold PBS for staining. In all cases, cells were stained in a 96-well U-bottom plate with Zombie Aqua fixable viability dye (1:1000) according to the manufacturer's instructions (Biolegend). Samples were then washed and resuspended in 50 μL cold FACS buffer (PBS, 2.5 mM EDTA, 2% FBS) containing TrueStain FcX™ block (Biolegend) for 10 min at 4 °C. Subsequently, cells were stained with antibodies (diluted 1:100) for 30 min at 4 °C in the dark. For experiments involving H-2K(b) chicken ova 257-264 SIINFEKL (AlexaFluor 647-labeled) tetramer, cells were stained with tetramer (diluted 1:1000) and antibodies (diluted 1:100) for 50 min at 4 °C in the dark. Finally, samples were washed twice and resuspended in 150 μL FACS buffer for acquisition on the Attune NxT flow cytometer (Life Technologies).

For flow cytometry on cell lines, adherent cells were rinsed once with sterile 1x PBS, and lifted by treating with 0.05% Trypsin-EDTA for 5 min. Trypsin was then neutralized with FACS buffer and cells were pelleted at 350 × g for 5 min at 4 °C, followed by resuspension in FACs buffer at a concentration of approximately $1{\times}10^6$ cells/mL. 50 μL of cells were then plated in a 96-well U-bottom plate and stained with antibodies (diluted 1:100) for 30 min at 4 °C in the dark. Finally, samples were washed twice and resuspended in 150 μL FACS buffer containing 1× DAPI (ThermoFisher, D1306) for acquisition on the Attune NxT flow cytometer (Life Technologies). Flow cytometry data was analyzed using FlowJo version 10.10.0.

Antibodies

The following antibodies were used for flow cytometry of mouse cell lines or tissue: anti-CD4 (Biolegend, 116012, clone RM4-4), anti-CD8a (Biolegend, 100722, clone 53-6.7), anti-CD45 (Biolegend, 103116, clone 30-F11), anti-CD11c (Biolegend, 117343, clone N418), anti-CD11b (Biolegend, 101228, clone M1/70), anti-MHCII I-A/I-E (Biolegend, 107618, clone M5/114.15.2), anti-CD69 (Biolegend, 104506, clone H1.2F3), anti-CD103 (Biolegend, 121408, clone 2E7), anti-CD80 (Biolegend, 104733, clone 16-10A1), anti-CD86 (Biolegend, 105013, clone GL-1), anti-CD45.2 (Biolegend, 109824, clone 104), anti-CD45R/B220 (Biolegend, 103207, clone RA3-6B2), anti-IFNAR1 (Biolegend, 127314, clone MAR1-5A3), TruStain FcX™ anti-CD16/32 (Biolegend, 101320, clone 93).

The following antibodies were used for flow cytometry of human cells or tissue: anti-CD141 (Thrombomodulin) (Biolegend, 344114, clone M80), anti-CD11c (Biolegend, 337210, clone Bu15), anti-HLA-DR (Biolegend, 327022, clone LN3), anti-CD14 (Biolegend, 982502, clone M5E2), anti-CD45 (Biolegend, 304058, clone HI30), anti-CD80 (Biolegend, 375410, clone W17149D), anti-CD86 (Biolegend, 374205, clone BU63), anti-HLA-A,B,C (Biolegend, 311406, clone W6/32), human TruStain FcX™ (Biolegend, 422302, Fc receptor blocking solution).

The following antibodies were used for ex vivo whole mount imaging or immunofluorescence microscopy: anti-Mac-2 (Galectin-3) (Biolegend, 125408, clone M3/38), anti-CD169 (Siglec-1) (Biolegend, 142404, clone 3D6.112), purified rat anti-mouse PNAd carbohydrate epitope (BD #553863), rabbit anti-GFP (ChromoTek, #pabg1), rabbit anti-mouse Lyve-1 (Cell Sciences, PA0846), AffiniPure Donkey anti-Rat IgG (H + L) AF647 (Jackson ImmunoResearch Labs, 712-605-150), AffiniPure Donkey anti-Rabbit IgG (H + L) Cy3 (Jackson ImmunoResearch Labs, 711-165-152).

The following antibodies were used for Western blot analysis: goat anti-mouse LDLR affinity purified polyclonal Ab (R&D systems, #AF2255), rabbit anti-LRPAP1 antibody (Sigma-Aldrich, #HPA008001), rabbit anti-α tubulin polyclonal antibody (Abcam, #ab18251), donkey anti-goat IgG HRP-conjugated antibody (R&D systems, #HAF109), Peroxidase AffiniPure goat anti-rabbit IgG (H + L) (Jackson Labs, #111-035-003).

The following antibodies were used for in vivo neutralization or depletion experiments: InVivoPlus anti-mouse PD-1 (CD279) (RMP1-14, BioXCell, #BE0146), InVivoPlus anti-mouse TNF (XT3.11, BioXCell, #BE0058), InVivoPlus anti-mouse IFNAR1 (MAR1-5A3, BioXCell, #BE0241), InVivoMab anti-mouse CD8α (2.43, BioXCell, #BE0061). Information related to antibodies can be found in Supplementary Table 2.

Adoptive transfer of Cell Trace Violet labeled OT-I cells

For OT-I CD8$^+$ T cell isolation, spleens and inguinal lymph nodes were harvested from OT-I mice and mashed through 70 μm cell strainers to generate single cell suspensions. Samples were then pelleted and splenocytes were subjected to red blood cell lysis using 1x RBC lysis buffer (for 5 min at RT). Single cell suspensions from spleens and lymph nodes were then pooled and CD8$^+$ T cells were isolated using the EasySep Mouse CD8$^+$ T cell Isolation Kit (StemCell Technologies, 19853). Finally, isolated CD8$^+$ T cells were labeled with CellTrace Violet (CTV, ThermoFisher, C34557) according to manufacturer's instructions. For adoptive transfer, CD45.1 mice were intravenously delivered 1.5×10^6 CTV-labeled OT-I cells in a 100 μL volume.

Quantification of virus particles in tissue or serum

Tumours, spleens or lymph nodes from mice infected with VSV$^{\Delta M51}$ were collected following euthanasia, and flash frozen in liquid nitrogen. When ready for titering, tissue samples were weighed, and added to gentleMACS D (Miltenyi Biotech) tubes containing 1 mL DMEM + 10% FBS. Tissue was then homogenized by running the gentleMACS on setting protein 01.01 for 60 s. Following this, the samples were pelleted at 300 × *g* for 5 min to collect the supernatant. This was then serially diluted in PBS and plated on Vero cells in 6-well plates. Infected Vero cells were cultured in DMEM medium supplemented with 10% FBS containing 1% carboxymethyl cellulose (Sigma-Aldrich, 21902) for 24 h, and then fixed and stained with crystal violet. Where possible, plaque counts were determined from wells containing 30–150 plaques. For titering virus in serum, blood was collected from mice infected with VSV$^{\Delta M51}$ via cardiac puncture and was allowed to clot undisturbed for 30 min at RT. Samples were then spun at 2000 × *g* for 10 min at 4 °C, and the resulting supernatant, designated serum, was collected for storage at −80 °C. When serum samples were ready for titering, they were serially diluted in PBS and plated on Vero cells in 6-well plates. Infected Vero cells were cultured in DMEM medium supplemented with 10% FBS containing 1% carboxymethyl cellulose for 24 h, and then fixed and stained with crystal violet. Where possible, plaque counts were determined from wells containing 30–150 plaques.

Bioluminescence imaging

For bioluminescence imaging of virus infection, mice were administered VSV$^{\Delta M51\text{-}oFluc}$ (5×10^8 PFU i.v., unless otherwise indicated). At indicated time points post-infection, animals were anesthetized with isoflurane and given D-luciferin i.p. (200 μL of 15 mg/mL, GoldBio, 115144-35-9). After 10 min, anesthetized mice were placed in nose cones within the imaging cabinet of the IVIS machine, and images were acquired using an IVIS Lumina machine (Perkin Elmer, Waltham, MA) on auto-exposure settings. For image analysis, data was processed using the Xenogen Living Image software. Using this software, a region of interest (ROI) was drawn over the area that was being monitored (either tumour or inguinal lymph node). This was followed by quantification of the average radiance (photons/s/cm^2/sr).

Serum transfer

Serum donors were first administered either PBS or VSV$^{\Delta M51}$ (5×10^8 PFU delivered i.v.) at 6 and 12 h before blood collection. Blood was then harvested via cardiac puncture and allowed to clot undisturbed at room temperature. After 30 min, samples were spun at 2000 × g for 10 min at 4 °C, and the resulting supernatant, designated serum, was collected into fresh Eppendorf tubes. Serum from each group was pooled to yield a single sample for control serum, serum collected 6 h post VSV$^{\Delta M51}$ administration, and serum collected 12 h post VSV$^{\Delta M51}$ administration. For serum transfer experiments, recipients received 200 μL of serum via intravenous delivery.

Suture of afferent lymphatic vessel draining popliteal lymph nodes

Afferent lymphatic vessels draining the popliteal lymph nodes were sutured as previously described[47]. Briefly, mice were anesthetized with an i.p. delivery of 250 μL of ketamine/xylazine (10 mg/mL ketamine and 1 mg/mL xylazine in saline). Both hindlimbs were then shaved, and 5 μL of 1% Evans blue was injected into each footpad to visualize afferent lymphatic vessels. For the afferent lymphatic suture: under a dissecting microscope, a small ~5 mm incision was made in the skin of the right hindleg, approximately 5 mm from the bottom edge of the popliteal fossa. Using fine operation forceps, the incision site was stretched slightly to expose the two afferent lymphatic vessels draining from the footpad to the popliteal lymph node. These vessels were then sutured shut using 0.7 metric monofilament polypropylene, and the skin incision was closed with sutures. For the sham surgery: under a dissecting microscope, a similar incision was made in the skin of the left hindleg, approximately 5 mm from the bottom edge of the popliteal fossa. Without disturbing the afferent lymphatic vessels, the skin incision was immediately closed with sutures. In most cases, mice were delivered PBS or 5×10^8–1×10^9 PFU VSV$^{\Delta M51}$ immediately after surgery.

Multiplex ELISA

For multiplex ELISA on lymph node homogenate, mouse lymph nodes were placed in pre-filled bead tubes (VWR, 10158-610) containing 175 μL of PBS with 1× protease inhibitor (Sigma-Aldrich, P8340) and 0.1% Tween20. Lymph nodes were then homogenized with a bead beater, pelleted at 10,000 × *g* for 10 min at 4 °C, and supernatant was harvested for cytokine analysis. For multiplex ELISA on serum, blood was harvested from mice via cardiac puncture and was allowed to clot undisturbed at room temperature. After 30 min, samples were spun at 2000 × *g* for 10 min at 4 °C, and the resulting supernatant, designated serum, was collected into fresh Eppendorf tubes. For Luminex bead-based multiplex array, cytokines/chemokines were detected using the commercially-available Mouse Cytokine/Chemokine 44-Plex Discovery Assay Array (MD44) from Eve Technologies (Calgary, AB Canada).

Splenectomy

For most splenectomy or sham surgeries, PBS or 5×10^8 PFU VSV$^{\Delta M51}$ was administered to mice 30 min prior to surgery. However, for studies testing the role of the spleen in immune checkpoint blockade, sham and splenectomy surgeries preceded treatment with anti-PD-1 and were carried out on mice bearing day 6 tumours, prior to the start of PBS or anti-PD-1 treatment. 5 min before the start of surgery, mice were anesthetized in a chamber using isoflurane (5% isoflurane, 1-2 L/min of oxygen), and delivered meloxicam (2 mg/kg) subcutaneously. Subsequently, the skin of the left upper abdomen was shaved and cleaned with depilatory cream. Mice were then transferred to a sterile field and placed in a nose cone to maintain anesthesia. The shaved area of the left abdomen was swabbed with iodine, and then a 5 mm incision was made under the rib cage, through the skin and peritoneum to expose the spleen. For splenectomy surgeries, the spleen was manipulated through the incision to sit outside the mouse. The blood vessels were then tied off with 5-0 Perma-Hand silk suture, and the spleen was removed. For both sham and splenectomy surgeries, the peritoneum was sutured closed using Vicryl. Finally, the skin was closed with 9 mm autoclips (stainless steel staples).

Analysis of human head and neck tumour samples

Fresh, surgically resected, head and neck squamous cell carcinoma tissues from four patients were provided by the Alberta Cancer Research Biobank under the approval of the Health Research Ethics Board of Alberta—Cancer Committee (reference number: HREBA.CC-16-0644). The samples were obtained with patient consent in

accordance with the principles of good clinical practice and the declaration of Helsinki. All four patients were lifelong non-smokers and had HPV-negative cancers: one 55-year-old female had a pT3N1 oral squamous cell carcinoma, one 73-year-old female had a pT2N3b oral squamous cell carcinoma, one 37-year-old female had a pT4aN0 sinonasal squamous cell carcinoma and one 77-year-old female had a pT4aN2b oral squamous cell carcinoma. Of the four patients, only the 55-year-old-female consumed alcohol (minimum consumption). Immediately after surgical resection, the samples were examined by the study pathologist and a ~10 mm^2 tumor fragment was transported to the lab for experimentation. There, tumour samples were embedded in 2% low-melting point agarose and sliced into 300 μm sections using a Leica VT1200S vibratome operating at 0.5 mm/s and a 1 mm amplitude. Tumour slices were then evenly distributed between two Millicell Cell Culture Inserts (Millipore, PIHP03050 0.4 μm, 30 mm diameter) placed in individual wells of a 6-well dish. Each well contained 1.5 mL DMEM + 10% FBS + 1% Antibiotic-Antimycotic (Gibco, 15240062). One well was left untreated, while the other received 50 ng/mL recombinant human IFN-β (PeproTech, AF-300-02B) and 20 ng/mL recombinant human TNF (PeproTech, AF-300-01A). 24 h post treatment, tumour slices were processed for flow cytometry. Tissues were first minced into pieces ~2-4 mm in diameter and placed into gentleMACs C tube (Miltenyi Biotech) containing 2.5 mL of digestion buffer (DMEM with 0.1 mg/mL Liberase TL, 0.05 mg/mL DNase I). The samples were then homogenized using the gentleMACS protocol h.imp.tumor.01, incubated for 45 min at 37 °C on a shaker, and then homogenized again using the gentleMACS protocol h.imp.tumor.01. Tumour cell suspensions were then strained through a 70 μM filter and pelleted at 350 × g for 5 min at 4 °C. Next, red blood cells were lysed by treating cells with 1× RBC lysis buffer (for 5 min at RT). Tumour cells were then pelleted at 350 × g for 5 min and resuspended in cold PBS. For staining, cells were transferred to a 96-well U-bottom plate and stained with Zombie Aqua fixable viability dye (1:1000) according to the manufacturer's instructions (Biolegend). Samples were then washed and resuspended in 50 μL cold FACS buffer containing human TrueStain FcX™ block (Biolegend) for 10 min at 4 °C. Subsequently, cells were stained with antibodies for 30 min at 4 °C in the dark. Finally, samples were washed twice and resuspended in 150 μL FACS buffer for acquisition on the Attune NxT flow cytometer (Life Technologies).

Statistical analysis

All statistical analyses were performed in GraphPad Prism v10 software. In all cases, $p < 0.05$ was considered a statistically significant difference. Data are shown as mean ± SD. Figure legends also contain the sample size (n) per experimental group, as well as the statistical tests implemented and post-hoc corrections. Unless otherwise indicated in the figure legend, measurements were taken from distinct samples. No statistical method was used to predetermine the sample size. No data were excluded from the analyses. Finally, investigators were not blinded during experiments and outcome analyses.

Reporting summary

Further information on research design is available in the Nature Portfolio Reporting Summary linked to this article.

Data availability

No large datasets were generated for this manuscript. All data are included in the main text, the Supplementary Information or are available from the authors, as are unique reagents used in this article. Source data—including the raw numbers for charts and graphs—are available in the Source Data file whenever possible. Source data are provided with this paper.

References

1. Lichty, B. D., Breitbach, C. J., Stojdl, D. F. & Bell, J. C. Going viral with cancer immunotherapy. *Nat. Rev. Cancer* **14**, 559–567 (2014).
2. Russell, S. J., Peng, K.-W. & Bell, J. C. Oncolytic virotherapy. *Nat. Biotechnol.* **30**, 658–670 (2012).
3. Liang, M. Oncorine, the world first oncolytic virus medicine and its update in China. *Curr. Cancer Drug Targets* **18**, 171–176 (2018).
4. Andtbacka, R. H. I. et al. Talimogene laherparepvec improves durable response rate in patients with advanced melanoma. *J. Clin. Oncol.* **33**, 2780–2788 (2015).
5. Todo, T. et al. Intratumoral oncolytic herpes virus G47Δ for residual or recurrent glioblastoma: a phase 2 trial. *Nat. Med.* **28**, 1630–1639 (2022).
6. Packiam, V. T. et al. An open label, single-arm, phase II multicenter study of the safety and efficacy of CG0070 oncolytic vector regimen in patients with BCG-unresponsive non–muscle-invasive bladder cancer: interim results. *Urol. Oncol. Semin. Orig. Investig.* **36**, 440–447 (2018).
7. Soliman, H. et al. Author Correction: oncolytic T-VEC virotherapy plus neoadjuvant chemotherapy in nonmetastatic triple-negative breast cancer: a phase 2 trial. *Nat. Med.* https://doi.org/10.1038/s41591-023-02309-4 (2023).
8. Cook, J. et al. Clinical activity of single-dose systemic oncolytic VSV virotherapy in patients with relapsed refractory T-cell lymphoma. *Blood Adv.* **6**, 3268–3279 (2022).
9. Diaz, R. M. et al. Oncolytic immunovirotherapy for melanoma using vesicular stomatitis virus. *Cancer Res.* **67**, 2840–2848 (2007).
10. Donnelly, O. G. et al. Measles virus causes immunogenic cell death in human melanoma. *Gene Ther.* **20**, 7–15 (2013).
11. Workenhe, S. T. & Mossman, K. L. Oncolytic virotherapy and immunogenic cancer cell death: sharpening the sword for improved cancer treatment strategies. *Mol. Ther. J. Am. Soc. Gene Ther.* **22**, 251–256 (2014).
12. Chen, D. S. & Mellman, I. Oncology meets immunology: the cancer-immunity cycle. *Immunity* **39**, 1–10 (2013).
13. Bommareddy, P. K., Zloza, A., Rabkin, S. D. & Kaufman, H. L. Oncolytic virus immunotherapy induces immunogenic cell death and overcomes STING deficiency in melanoma. *Oncoimmunology* **8**, 1591875 (2019).
14. Ma, J. et al. Characterization of virus-mediated immunogenic cancer cell death and the consequences for oncolytic virus-based immunotherapy of cancer. *Cell Death Dis.* **11**, 48 (2020).
15. Workenhe, S. T. et al. Immunogenic HSV-mediated oncolysis shapes the antitumor immune response and contributes to therapeutic efficacy. *Mol. Ther. J. Am. Soc. Gene Ther.* **22**, 123–131 (2014).
16. Flores, E. B. & Bartee, E. Decreasing the susceptibility of malignant cells to infection does not impact the overall efficacy of myxoma virus-based oncolytic virotherapy. *Mol. Ther. Oncolytics* **19**, 323–331 (2020).
17. Galivo, F. et al. Single-cycle viral gene expression, rather than progressive replication and oncolysis, is required for VSV therapy of B16 melanoma. *Gene Ther.* **17**, 158–170 (2010).
18. Prestwich, R. J. et al. Immune-mediated antitumor activity of reovirus is required for therapy and is independent of direct viral oncolysis and replication. *Clin. Cancer Res.* **15**, 4374–4381 (2009).
19. Ricca, J. M. et al. Pre-existing immunity to oncolytic virus potentiates its immunotherapeutic efficacy. *Mol. Ther. J. Am. Soc. Gene Ther.* **26**, 1008–1019 (2018).
20. Leddon, J. L. et al. Oncolytic HSV virotherapy in murine sarcomas differentially triggers an antitumor T-cell response in the absence of virus permissivity. *Mol. Ther. Oncolytics* **1**, 14010 (2015).
21. Arulanandam, R. et al. VEGF-mediated induction of PRD1-BF1/Blimp1 expression sensitizes tumor vasculature to oncolytic virus infection. *Cancer Cell* **28**, 210–224 (2015).

22. Breitbach, C. J. et al. Targeting tumor vasculature with an oncolytic virus. *Mol. Ther. J. Am. Soc. Gene Ther.* **19**, 886–894 (2011).
23. Chakrabarty, R. et al. Bio-distribution study of Reolysin® (pelareorep) through a single intravenous infusion in Sprague-Dawley rats. *Invest. New Drugs* **31**, 1476–1486 (2013).
24. Peng, K.-W. et al. Biodistribution of oncolytic measles virus after intraperitoneal administration into Ifnar-CD46Ge transgenic mice. *Hum. Gene Ther.* **14**, 1565–1577 (2003).
25. Pol, J. G. et al. Preclinical evaluation of a MAGE-A3 vaccination utilizing the oncolytic Maraba virus currently in first-in-human trials. *Oncoimmunology* **8**, e1512329 (2018).
26. Bridle, B. W. et al. Privileged antigen presentation in splenic B cell follicles maximizes T cell responses in prime-boost vaccination. *J. Immunol.* **196**, 4587–4595 (2016).
27. Honke, N. et al. Enforced viral replication activates adaptive immunity and is essential for the control of a cytopathic virus. *Nat. Immunol.* **13**, 51–57 (2011).
28. Naumenko, V. et al. Visualizing oncolytic virus-host interactions in live mice using intravital microscopy. *Mol. Ther. Oncolytics* **10**, 14–27 (2018).
29. Kim, D.-S. et al. Smac mimetics and oncolytic viruses synergize in driving anticancer T-cell responses through complementary mechanisms. *Nat. Commun.* **8**, 344 (2017).
30. Breitbach, C. J. et al. Oncolytic vaccinia virus disrupts tumor-associated vasculature in humans. *Cancer Res.* **73**, 1265–1275 (2013).
31. Ruotsalainen, J. J. et al. Clonal variation in interferon response determines the outcome of oncolytic virotherapy in mouse CT26 colon carcinoma model. *Gene Ther.* **22**, 65–75 (2015).
32. Breitbach, C. J. et al. Targeted inflammation during oncolytic virus therapy severely compromises tumor blood flow. *Mol. Ther.* **15**, 1686–1693 (2007).
33. Finkelshtein, D., Werman, A., Novick, D., Barak, S. & Rubinstein, M. LDL receptor and its family members serve as the cellular receptors for vesicular stomatitis virus. *Proc. Natl. Acad. Sci. USA.* **110**, 7306–7311 (2013).
34. Chen, C.-Y. et al. Cooperation of oncolytic herpes virotherapy and PD-1 blockade in murine rhabdomyosarcoma models. *Sci. Rep.* **7**, 2396 (2017).
35. Granot, T., Yamanashi, Y. & Meruelo, D. Sindbis viral vectors transiently deliver tumor-associated antigens to lymph nodes and elicit diversified antitumor CD8+ T-cell immunity. *Mol. Ther. J. Am. Soc. Gene Ther.* **22**, 112–122 (2014).
36. Meadors, J. L. et al. Murine rhabdomyosarcoma is immunogenic and responsive to T-cell-based immunotherapy. *Pediatr. Blood Cancer* **57**, 921–929 (2011).
37. Hildebrand, K. M. et al. The KrasG12D;Trp53fl/fl murine model of undifferentiated pleomorphic sarcoma is macrophage dense, lymphocyte poor, and resistant to immune checkpoint blockade. *PloS One* **16**, e0253864 (2021).
38. Klein, S. L. & Flanagan, K. L. Sex differences in immune responses. *Nat. Rev. Immunol.* **16**, 626–638 (2016).
39. Katze, M. G., He, Y. & Gale, M. Viruses and interferon: a fight for supremacy. *Nat. Rev. Immunol.* **2**, 675–687 (2002).
40. Zhi, L. et al. FTY720 blocks egress of T cells in part by abrogation of their adhesion on the lymph node sinus. *J. Immunol.* **187**, 2244–2251 (2011).
41. Salmon, H. et al. Expansion and activation of CD103(+) dendritic cell progenitors at the tumor site enhances tumor responses to therapeutic PD-L1 and BRAF inhibition. *Immunity* **44**, 924–938 (2016).
42. Hildner, K. et al. Batf3 deficiency reveals a critical role for CD8alpha+ dendritic cells in cytotoxic T cell immunity. *Science* **322**, 1097–1100 (2008).
43. Dammeijer, F. et al. The PD-1/PD-L1-checkpoint restrains T cell immunity in tumor-draining lymph nodes. *Cancer Cell* **38**, 685–700.e8 (2020).
44. Francis, D. M. et al. Blockade of immune checkpoints in lymph nodes through locoregional delivery augments cancer immunotherapy. *Sci. Transl. Med.* **12**, eaay3575 (2020).
45. Macatonia, S. E., Knight, S. C., Edwards, A. J., Griffiths, S. & Fryer, P. Localization of antigen on lymph node dendritic cells after exposure to the contact sensitizer fluorescein isothiocyanate. Functional and morphological studies. *J. Exp. Med.* **166**, 1654–1667 (1987).
46. Iannacone, M. et al. Subcapsular sinus macrophages prevent CNS invasion on peripheral infection with a neurotropic virus. *Nature* **465**, 1079–1083 (2010).
47. Lin, Y., Xue, J. & Liao, S. Blocking lymph flow by suturing afferent lymphatic vessels in mice. *J. Vis. Exp. JoVE* https://doi.org/10.3791/61178 (2020).
48. Fuertes, M. B. et al. Host type I IFN signals are required for antitumor CD8+ T cell responses through CD8{alpha}+ dendritic cells. *J. Exp. Med.* **208**, 2005–2016 (2011).
49. Trevejo, J. M. et al. TNF-α-dependent maturation of local dendritic cells is critical for activating the adaptive immune response to virus infection. *Proc. Natl. Acad. Sci.* **98**, 12162–12167 (2001).
50. Fuertes Marraco, S. A. et al. Novel murine dendritic cell lines: a powerful auxiliary tool for dendritic cell research. *Front. Immunol.* **3**, 331 (2012).
51. Canton, J. et al. The receptor DNGR-1 signals for phagosomal rupture to promote cross-presentation of dead-cell-associated antigens. *Nat. Immunol.* **22**, 140–153 (2021).
52. Gros, M. et al. Endocytic membrane repair by ESCRT-III controls antigen export to the cytosol during antigen cross-presentation. *Cell Rep.* **40**, 111205 (2022).
53. Biesmans, S. et al. Peripheral administration of tumor necrosis factor-alpha induces neuroinflammation and sickness but not depressive-like behavior in mice. *BioMed. Res. Int.* **2015**, 716920 (2015).
54. Skelly, D. T., Hennessy, E., Dansereau, M.-A. & Cunningham, C. A systematic analysis of the peripheral and CNS effects of systemic LPS, IL-1B, TNF-α and IL-6 challenges in C57BL/6 mice. *PLoS One* **8**, e69123 (2013).
55. Stifter, S. A. et al. Visualizing the selectivity and dynamics of interferon signaling in vivo. *Cell Rep.* **29**, 3539–3550.e4 (2019).
56. van Holten, J. et al. Treatment with recombinant interferon-beta reduces inflammation and slows cartilage destruction in the collagen-induced arthritis model of rheumatoid arthritis. *Arthritis Res. Ther.* **6**, R239–R249 (2004).
57. Antonio, N. et al. The wound inflammatory response exacerbates growth of pre-neoplastic cells and progression to cancer. *EMBO J.* **34**, 2219–2236 (2015).
58. Oseledchyk, A. et al. Lysis-independent potentiation of immune checkpoint blockade by oncolytic virus. *Oncotarget* **9**, 28702–28716 (2018).
59. Wongthida, P. et al. VSV oncolytic virotherapy in the B16 model depends upon intact MyD88 signaling. *Mol. Ther. J. Am. Soc. Gene Ther.* **19**, 150–158 (2011).
60. Flick, D. A. & Gifford, G. E. Pharmacokinetics of murine tumor necrosis factor. *J. Immunopharmacol.* **8**, 89–97 (1986).
61. SALMON, P., LE COTONNEC, J.-Y., GALAZKA, A., ABDUL-AHAD, A. & DARRAGH, A. Pharmacokinetics and pharmacodynamics of recombinant human interferon-β in healthy male volunteers. *J. Interferon Cytokine Res.* **16**, 759–764 (1996).
62. Zhang, K.-J. et al. A potent in vivo antitumor efficacy of novel recombinant type I interferon. *Clin. Cancer Res.* **23**, 2038–2049 (2017).

63. Barchet, W. et al. Virus-induced interferon alpha production by a dendritic cell subset in the absence of feedback signaling in vivo. *J. Exp. Med.* **195**, 507–516 (2002).
64. Kim, M. et al. Amplification of oncolytic vaccinia virus widespread tumor cell killing by sunitinib through multiple mechanisms. *Cancer Res.* **78**, 922–937 (2018).
65. Selman, M. et al. Multi-modal potentiation of oncolytic virotherapy by vanadium compounds. *Mol. Ther. J. Am. Soc. Gene Ther.* **26**, 56–69 (2018).
66. Wedge, M.-E. et al. Virally programmed extracellular vesicles sensitize cancer cells to oncolytic virus and small molecule therapy. *Nat. Commun.* **13**, 1898 (2022).
67. Sivanandam, V., LaRocca, C. J., Chen, N. G., Fong, Y. & Warner, S. G. Oncolytic viruses and immune checkpoint inhibition: the best of both worlds. *Mol. Ther. Oncolytics* **13**, 93–106 (2019).
68. Kepp, O., Zitvogel, L. & Kroemer, G. Clinical evidence that immunogenic cell death sensitizes to PD-1/PD-L1 blockade. *Oncoimmunology* **8**, e1637188 (2019).
69. Barnard, Z. et al. Expression of FMS-like tyrosine kinase 3 ligand by oncolytic herpes simplex virus type I prolongs survival in mice bearing established syngeneic intracranial malignant glioma. *Neurosurgery* **71**, 741–748 (2012).
70. Svensson-Arvelund, J. et al. Expanding cross-presenting dendritic cells enhances oncolytic virotherapy and is critical for long-term anti-tumor immunity. *Nat. Commun.* **13**, 7149 (2022).
71. Evans, R., Kamdar, S. J., Duffy, T. & Edison, L. Intratumor gene expression after adoptive immunotherapy in a murine tumor model. Regulation of messenger RNA levels associated with the differential expansion of tumor-infiltrating lymphocytes. *J. Immunol.* **150**, 177–184 (1993).
72. Karttunen, J., Sanderson, S. & Shastri, N. Detection of rare antigen-presenting cells by the lacZ T-cell activation assay suggests an expression cloning strategy for T-cell antigens. *Proc. Natl. Acad. Sci. USA.* **89**, 6020–6024 (1992).
73. Stojdl, D. F. et al. VSV strains with defects in their ability to shutdown innate immunity are potent systemic anti-cancer agents. *Cancer Cell* **4**, 263–275 (2003).
74. Potts, K. G. et al. Deletion of F4L (ribonucleotide reductase) in vaccinia virus produces a selective oncolytic virus and promotes anti-tumor immunity with superior safety in bladder cancer models. *EMBO Mol. Med.* **9**, 638–654 (2017).
75. Turk, M., Naumenko, V., Mahoney, D. J. & Jenne, C. N. Tracking cell recruitment and behavior within the tumor microenvironment using advanced intravital imaging approaches. *Cells* **7**, 69 (2018).

Acknowledgements

The authors thank Dr. David Stojdl (CHEO), Dr. David Evans (U. Alberta) and Dr. Crystal MacKall (Stanford) for providing OV strains and cell lines. The authors additionally thank the NIH Tetramer Core Facility (contract number 75N93020D00005) for providing H-2K(b) chicken ova 257-264 SIINFEKL tetramers. Finally, the authors thank the following funding sources: Canadian Institutes of Health Research Grant 420828 (D.J.M., C.N.J.); Vanier Canada Graduate Scholarship 433550 (J.R.); Alberta Children's Hospital Foundation Grant ACHF21-0845 (D.J.M.); Canadian Cancer Society Research Institute ACTION-20 (D.J.M.); Canadian Institutes of Health Project Grant 156035 (S.L.); Canadian Cancer Society Research Training Award 707979 (S.S.) and 707977 (L.K.M.); Terry Fox Research Institute Grant 1151-06 (L.K.M.).

Author contributions

Conceptualization: J.R., V.N., F.J.Z., K.C.K.L., D.J.M. Methodology: J.R., V.N., C.G., F.J.Z., D.J.M. Investigation: J.R., D.V., M.T., D.S.K., S.S, L.K.M., G.A.G., J.X., A.C., K.P., H.T., M.H., K.M.H. Visualization: J.R., F.J.Z. Funding acquisition: J.R., D.J.M., S.L., C.N.J. Project administration: F.J.Z., D.J.M. Supervision: F.J.Z., J.A.C., M.J.M., P.B., S.L., C.N.J., J.C., D.J.M. Writing—original draft: J.R., F.J.Z., D.J.M. All authors read and approved the manuscript.

Competing interests

The authors declare no competing interests.

Additional information

Supplementary information The online version contains supplementary material available at https://doi.org/10.1038/s41467-024-54111-6.

Correspondence and requests for materials should be addressed to Douglas J. Mahoney.

Peer review information *Nature Communications* thanks Dorothee von Laer and the other anonymous reviewer(s) for their contribution to the peer review of this work. A peer review file is available.